TU Delft

Delft University of Technology

InP colloidal quantum dots for visible and near-infrared photonics

Almeida, Guilherme; Ubbink, Reinout F.; Stam, Maarten; du Fossé, Indy; Houtepen, Arjan J.

DOI
10.1038/s41578-023-00596-4

Publication date
2023

Document Version
Final published version

Published in
Nature Reviews Materials

Citation (APA)
Almeida, G., Ubbink, R. F., Stam, M., du Fossé, I., & Houtepen, A. J. (2023). InP colloidal quantum dots for visible and near-infrared photonics. *Nature Reviews Materials*, *8*(11), 742-758. https://doi.org/10.1038/s41578-023-00596-4

Important note
To cite this publication, please use the final published version (if applicable).
Please check the document version above.

Copyright
Other than for strictly personal use, it is not permitted to download, forward or distribute the text or part of it, without the consent of the author(s) and/or copyright holder(s), unless the work is under an open content license such as Creative Commons.

Takedown policy
Please contact us and provide details if you believe this document breaches copyrights.
We will remove access to the work immediately and investigate your claim.

This work is downloaded from Delft University of Technology.
For technical reasons the number of authors shown on this cover page is limited to a maximum of 10.

Green Open Access added to TU Delft Institutional Repository

'You share, we take care!' - Taverne project

https://www.openaccess.nl/en/you-share-we-take-care

Otherwise as indicated in the copyright section: the publisher is the copyright holder of this work and the author uses the Dutch legislation to make this work public.

nature reviews materials

https://doi.org/10.1038/s41578-023-00596-4

Review article

Check for updates

InP colloidal quantum dots for visible and near-infrared photonics

Guilherme Almeida ✉, Reinout F. Ubbink, Maarten Stam, Indy du Fossé & Arjan J. Houtepen ✉

Abstract

Owing to their tunable band gap, high absorption coefficient, narrow emission linewidths and unrestricted composition, InP-based colloidal quantum dots (QDs) have become industrially relevant for visible and near-infrared photonic technologies. Although their development has so far been strongly driven by their suitability for green and red light-emitting diodes, the spectrum of applications for this class of materials is much broader. This Review covers the multidisciplinary field of InP-based QDs from its genesis in the mid-1990s to date, drawing on relevant knowledge from other classes of QDs and from III–V semiconductors as a whole. We discuss the optoelectronic properties of InP QDs, their fabrication, their defects and passivation strategies and the design of InP-based QD heterostructures. Finally, we outline the technological status of these QDs for various photonic applications.

Sections

Applied Science, TU Delft, Delft, Netherlands. ✉e-mail: almeida.guilherme@gmail.com; a.j.houtepen@tudelft.nl

Introduction

Semiconductor technologies have revolutionized our civilization over the past 50 years, in particular through electronic and photonic applications. A well-known feature of semiconductors is that their electronic and optical properties depend not only on their composition and structure but also on their size and shape when confined to the nanometre scale, owing to quantum mechanical effects[1–6]. By virtue of their tunable energy landscapes, quantized signatures and efficient luminescence, semiconductor nanostructures (also known as quantum dots (QDs), wires or wells) have been widely explored at a fundamental level and can be found in electronic and photonic technologies as common as transistors or light-emitting diodes (LEDs).

Surfactant-assisted syntheses of colloidal nanocrystals have enabled the fabrication of an enormous variety of semiconductor nanostructures with remarkable precision in terms of composition, structure and morphology and in high yields[7–11]. Their freestanding colloidal form also confers great versatility for further integration into devices. As the design, stability, performance and functionality of colloidal QDs, wires and wells have evolved over the past three decades, they have become valuable materials for a growing number of photonic technologies such as lighting, displays, lasers, quantum information, solar energy converters, infrared cameras, security inks and theranostics[11–25].

InP-based colloidal QDs have raised considerable interest for photonic technologies operating in the visible and near-infrared (NIR) regions, because of their wide spectral tunability, strong light absorption, efficient luminescence, high carrier mobility and compliance with safety regulations on consumer devices. Advances in their synthesis and design have considerably improved their quality[26,27]. InP-based QDs can already be found integrated as down-converting phosphors in commercial lamps and displays[28,29] and are being considered for other applications as their qualities improve and expand, such as for gain media or NIR light sources and detectors.

In this Review, we discuss the growing field of InP-based QDs from its genesis in the mid-1990s to date, providing a comprehensive but concise account of its progress and challenges and drawing on relevant knowledge from other types of QDs and from III–V semiconductors as a whole for a more complete picture. We cover the electronic and optical properties of InP QDs, their synthesis and the occurrence and passivation of electronic defects. We also examine the types of QD heterostructures on the basis of InP and examine the various photonics applications of these systems. While writing this article it became apparent to us, as it will to the reader, that the large body of literature on InP QDs is not always coherent, owing to the structural complexity that these systems can have. Therefore, we also critically cross-analyse the literature to provide structure, clarity and guidance to the field. Finally, we highlight the research directions that we believe will advance knowledge and applicability of this class of QDs.

General properties of InP

InP is a semiconductor that usually crystallizes in the zinc-blende structure. It is considered a relatively covalent semiconductor and has a direct band gap of approximately 1.35 eV in its bulk form[30] (Table 1). The band gap is formed between valence orbitals with bonding character and conduction orbitals with antibonding character. Specifically, the valence band edge of InP is characterized by a strong contribution from P 3*p* orbitals, whereas the conduction band edge has a more mixed character, with the largest contribution coming from the In 5*s* orbitals, as well as a lower density of states[31] (Fig. 1a). Its band structure is characterized by direct transitions from light, heavy and split-off hole states[32–34], and its absorption coefficient is relatively strong (>10^4 cm^{-1} at 1.4 eV) (Fig. 1b).

Owing to the quantum size effect[1–6], the band gap of InP can be tuned from the NIR (1.3 eV) up to the violet (approximately 2.7 eV) by confining InP to a fraction of its Bohr radius (around 10 nm). The relationship between band gap and volume for InP QDs[35] is reported in Fig. 1c. Although the individual band edge shifts are not fully established, it has been suggested that the conduction band levels are more sensitive to quantum confinement than are the valence levels, based on simple effective mass arguments and confirmed by more advanced computations (see Table 1 for effective masses)[36–38].

At room temperature, luminescence linewidths of approximately 50 meV have been observed from a single InP QD emitting in the red and around 80 meV for smaller green-emitting dots[35] (Fig. 1d). For applications such as displays, narrow emission linewidths from QD ensembles are required. Although the emission linewidth of a single QD is size-dependent and limited by ultrafast structural dynamics and electron–phonon coupling[39–47], which are, in turn, exacerbated by the presence of electronic traps[48,49], the linewidths of an ensemble of QDs are further broadened by its size distribution. Narrower linewidths may be obtainable in QDs with higher quantum yields as well as in core–shell structures.

We note that in QDs, the electron–hole exchange interaction causes the splitting of degenerate electron–hole pair configurations into various states[50]. Briefly, in zinc-blende QDs such as InP, the conduction band edge is formed by a double degenerate electron level, whereas the valence band edge is formed by a fourfold degenerate hole level. Exchange interactions between these levels, combined with shape anisotropy, give rise to an exciton fine structure, with an $F = \pm 2$ dark lowest exciton state, separated by 2–9 meV from an $F = \pm 1$ bright state (depicted in the inset of Fig. 1d, data from core–shell QDs)[50–52]. At room temperature, the emission comes from the thermally populated high energy bright exciton state. In principle, this fine-structure splitting is similar to that observed in other tetrahedral binary semiconductors such as CdSe. However, it has been shown that the fine structure in InP QDs is particularly insensitive to shape anisotropy. This phenomenon is attributed to the particular ratio of the light hole over the heavy hole effective mass[52,53]. In InP, this ratio is 0.15, close to the value of 0.14, in which the exciton fine structure is predicted to be least sensitive to shape anisotropy[54]. As a consequence, the exciton remains nearly isotropic even for prolate or oblate InP QDs. This explains why mixing of the low energy dark exciton with the higher energy bright exciton does not occur in magnetic fields[53], and why the bright exciton is found to consist of a doublet in single-particle cryogenic photoluminescence measurements[52].

The luminescence of QDs is typically limited by electronic traps arising from structural defects and also by Auger processes that take place in the multi-exciton and charged regimes (of relevance for applications such as LEDs or lasers)[13,55]. There has been great progress in mitigating trap-related losses in InP QDs but much less so in solving Auger losses. Non-radiative Auger processes are extremely relevant as InP QDs emitting in the visible exhibit bi-exciton lifetimes of 5–60 ps, three to four orders of magnitude shorter than the single exciton lifetime[35]. In addition, Auger processes produce energetic carriers that can lead to irreversible redox chemistry and device degradation.

Finally, particular applications (such as coherent single-photon emission) require QDs with relatively long coherence times. Although it is known that the coherence times of QDs can be limited by

Table 1 | Structural, mechanical and optoelectronic properties of selected bulk semiconductors in the zinc-blende or wurtzite (w) structure[365–370]

Material	*a* (A)	E_g (eV)	E_{VB} (eV)	DOS (VB) (states per eV)	DOS (CB) (states per eV)	m_e	m_h (lh/hh)	α (2.5 eV) ($\times 10^5$ cm^{-1})	T_D (K)	B_s (GPa)	PI
InN (w)	3.53/5.69	2	6.43	5.3×10^{19}	9.0×10^{17}	0.11	0.27/1.63	1.21	660	140	
GaP	5.45	2.26	5.51	1.9×10^{19}	1.8×10^{19}	1.12/0.22	0.14/0.79	0.01	445	88	0.33
InP	5.87	1.34	5.17	1.1×10^{19}	5.7×10^{17}	0.08	0.6/0.089	1.30	425	71	0.42
GaAs	5.65	1.42	4.98	9.0×10^{17}	4.7×10^{17}	0.063	0.51/0.082	0.99	360	75	0.31
InAs	6.06	0.35	4.69	6.6×10^{18}	8.7×10^{16}	0.023	0.41/0.026	4.53	280	58	0.36
CdSe	4.30	1.7	4.75			0.13	0.45	1.21			0.70
ZnSe	5.67	2.82	5.98			0.14	0.6	–			0.63
ZnS	5.41	3.68	6.53			0.28	–	–			0.62

Lattice constant (*a*), band gap (E_g), valence band energy (E_{VB}) versus vacuum, effective density of states (DOS) at the valence band (VB) and conduction band (CB), effective mass of electrons (m_e) and holes (m_h), absorption coefficient (α) at 2.50 eV, Debye temperature (T_D), bulk modulus (B_s) and the Phillips iconicity (PI, a larger or smaller value characterizes a more ionic or more covalent lattice, respectively). For GaP, two m_e values are given (longitudinal and transversal) because the surfaces of equal energies are ellipsoids. lh, light hole; hh, heavy hole.

structural dynamics and electron–phonon coupling[39,41,56,57], and also by fine-structure-related transitions[50,58–60], no studies of the coherence time have been conducted on InP QDs.

Although we discuss the relationship between structure and optoelectronic properties of InP-based QDs in the following sections, we note that this link is not always straightforward to assess. The QDs in ensembles are not all exactly the same in terms of size, shape, composition, structure and surface coverage, which leads to a distribution in optoelectronic properties. In addition, there are difficulties inherent to physical characterization at such small scales.

Synthesis of colloidal InP QDs

Various protocols have been proposed to synthesize InP QDs[61–80]. InP QDs are generally produced by reacting an In^{3+} salt with a P^{3-} source in a liquid medium and in the presence of ions and/or molecules (termed ligands) that bind to the surface of QDs, providing colloidal stability. Alternatively, the P^{3-} ion may also be formed in situ by reducing a phosphorus compound in a higher oxidation state. Of all the methods, two surfactant-assisted syntheses in nonpolar solvents have become the most popular and are currently used in industrial-scale manufacturing.

In one synthesis (Fig. 2a, top), indium (III) alkanoates of general formula $In(RCOO)_3$ (R = alkylic chain, typically C_{14-18}) are reacted with an organic silyl phosphine of general formula $P(SiR_3)_3$ (R = alkyl or aryl, typically CH_3) at temperatures up to 300 °C (refs. 64,81–84). This path leads to QDs capped by alkanoates (whether SiR_3 groups are also present on the surface remains unclear)[85]. When this synthesis is carried out at more elevated temperatures, it delivers the most monodisperse InP QDs of all methods, and impressively narrow linewidths can be obtained by adding trioctylphosphine to the synthesis[72–74] (Fig. 2b,c). However, this route is prone to several unwanted side reactions. For instance, free carboxylic acids left from the preparation of the indium alkanoate precursor can react with the formed InP QDs, producing PH_3 (ref. 86); react with $P(SiR_3)_3$, leading to a series of phosphorus precursors of varying reactivities[87,88]; or condense into ketones, releasing water molecules that can then oxidize the InP QDs and/or react with indium alkanoates to form In_2O_3 particles[85,89]. These side reactions can be suppressed by adding a base (such as trioctylphosphine), keeping the temperature low, or purifying the indium alkanoate precursor. Nevertheless, even with these adjustments, indium alkanoates themselves may be prone to other side reactions[90]. In addition, the silyl phosphine precursors used are pyrophoric, making them hard to handle and expensive.

The other common route (Fig. 2a, middle) is based on the reaction of indium (III) halides (typically $InCl_3$) with aminophosphines of general formula $P(HNR)_3$ (typically formed in situ by the reaction of primary alkyl amines RNH_2 with $P(NR_2)_3$ precursors). The aminophosphines act simultaneously as a P-source (in an oxidation state of +3) and as a reducing agent (to reduce P to −3)[76–78]. This method forms QDs capped by halide ions and alkylamines. Alternatively, indium (I) halides and/or PX_3 (X = Cl, Br or I) may be used as precursors[91–93]. Compared with the first route, this route has been less studied and cannot yet produce QDs as monodisperse[94], but it is definitely more cost-attractive owing to its cheaper precursors.

It is not well understood how the different chemicals used in each of these synthetic routes affect the growth mechanism, reaction kinetics or morphology of the resulting InP QDs. Studying the growth kinetics has long been complicated by oxidation of InP QDs during the synthesis, which was only recently circumvented by using reducing atmospheres[95–97]. Nevertheless, it is known that the growth of InP QDs using indium carboxylates and $P(SiR_3)_3$ precursors proceeds through the formation and ripening of cluster intermediates[98–104] whose structure has been identified[105] and also that these clusters can be used as single-source precursors for synthesizing InP QDs[73,99]. Other noteworthy advances include preliminary studies on the determination and control of reaction kinetics using various aminophosphines[106], the investigation of nucleation and growth through computational methods[107] and the successful development of continuous production methods[108–114].

Shape-wise, both routes yield InP QDs that appear in electron micrographs to adopt a triangular pyramidal shape (Fig. 2d). Large InP QDs synthesized by the aminophosphine route have been found to derive their eventual tetrahedral shape from smaller, early-stage tetrapod InP QDs whose arms are enclosed by (110) facets[115]. Interestingly, the tetrapod shape could be controlled to a certain degree by controlling the reaction temperature and amount of precursors. The experimentally observed tetrahedral shape has been rationalized as fulfilling the requirement of charge neutrality with common monovalent ligands, such that (100) facets are unlikely to be expressed in cation-rich InP QDs and a (111) termination is more favourable[38]. Following this

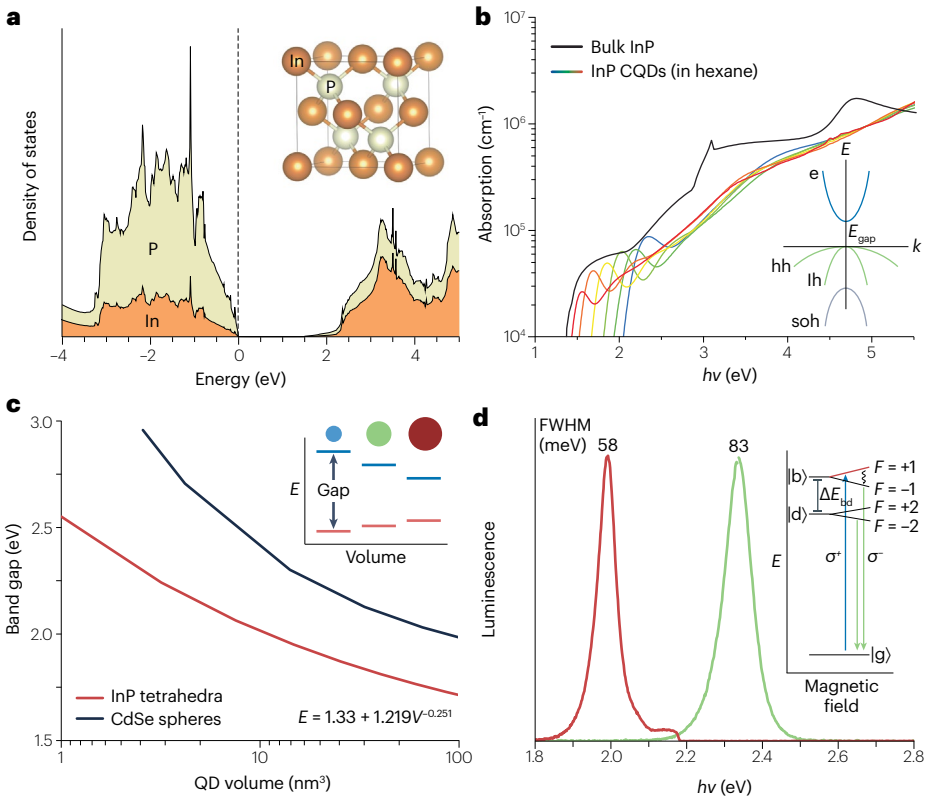

Fig. 1 | Optoelectronic properties of InP. a, Bulk density of states. The inset shows the zinc-blende unit cell. **b**, Absorption coefficients of bulk InP and of InP colloidal quantum dots (CQDs) with edge lengths ranging from 1.5 nm to 4.0 nm. The inset shows the simplified band structure. **c**, Band gap versus QD volume. The inset illustrates the shift of the band edge levels of InP with quantum confinement. **d**, Room-temperature photoluminescence spectra of single InP QD emitting in the red and in the green exhibiting full widths at half maximum (FWHM) of approximately 58 meV and 83 meV, respectively. The inset shows fine structure splitting at 4 K. lh, light hole; hh, heavy hole; soh, split-off hole. Panel **a** adapted from ref. 31, Springer Nature Limited. Panels **b**–**d** adapted with permission from ref. 35. Copyright 2023 American Chemical Society. Inset in panel **d** adapted with permission from ref. 51, ACS.

line of reasoning, other possible shapes include truncated pyramids and small-sized cuboctahedrons with (100), (111) and (−111) facets. Density-functional theory calculations also show that both bare and ligand-terminated (111) facets exhibit a lower surface energy than (100) facets[116].

Ga-substituted and As-substituted alloys of InP QDs can also be synthesized using variations of the aforementioned routes[117–121]. However, control over morphology and structure of InP-based QDs through direct synthesis remain a challenge[122]. Nonetheless, morphology-controlled InP QDs can still be prepared indirectly, by transforming (cation-exchanging) other metal phosphide nanocrystals into InP QDs while preserving the original phase and morphology (Fig. 2a, bottom). In this way, hexagonal (wurtzite) InP platelets (Fig. 2e) and InP rods could be successfully prepared from their Cu_3P analogues[123–126]. Control over the exchange rate is important to ensure that single crystalline InP QDs are obtained[124].

Surface ligands have a key role not only in the synthesis, colloidal stability and self-assembly of QDs but also in many of their optoelectronic properties (such as trap passivation, electron–phonon coupling, carrier delocalization and film conductivity). Ligands also enable post-synthetic surface functionalization. In fact, surface-ligand engineering of QDs has been intensely investigated[121,127,128] and reviewed[10,129–131].

Defects and trap passivation

As-synthesized InP QDs typically exhibit weak luminescence efficiencies, of a few percent at most (often <1%). Defect passivation and shelling approaches allow QDs to be prepared with near-unity efficiencies. Various types of defects are possible in InP materials in general (including QDs and thin films), but can be passivated and mitigated with several strategies (Fig. 3).

Oxidation and etching

III–V semiconductors, including InP, are prone to oxidation, which limits their growth and luminescence efficiency[74,96,132–140]. Oxygen is known to adsorb dissociatively on (bulk) InP surfaces[141–144], and at room temperature In-O-P and PO_x species ($x > 1$) form at oxygen pressures as low as 5 µbar and 5 mbar, respectively, highlighting the strong reactivity of the phosphide anion towards oxidation. Further structural transformations occur at higher temperatures, including the bridging of PO_x units at around 200 °C and the development of a thick indium oxide layer above 300 °C, underlining the diffusion of oxygen[143,145]. Water also appears to adsorb dissociatively[143,146] and to lead to In-O-P and PO_x species on mild heating (100 °C). In-O-In species can also form, more likely on exposure to oxygen than to water[143].

This tendency to oxidize poses difficulties for the synthesis (and shelling) of InP QDs[87,89,95,147,148], and indeed hydroxyl groups[149] and oxidized phosphorus have been identified on these QDs[85,135,136,138,150,151] (Fig. 3, 1–4). The sources of oxidation and types of oxidative defects are likely various, and their impacts on the electronic structure of InP QDs remain unclear. The absence of oxidized species often appears to be correlated with increased luminescence efficiency[74,136–138,140,152], although opposite results have also been observed[147,153–159].

Computational studies are especially suitable to elucidate the effects of oxidation, even though research has mainly been limited to flat (001) surfaces without ligands[142,145,160–164]. Some of these studies report the appearance of trap states upon oxidation[142,145,160,164,165], but the underlying mechanisms that lead to trap formation are not entirely

understood. For example, one study reported that only substitutional oxygen atoms, but not In-O-P and In-O-In moieties formed by oxygen adsorption, produced trap states[142]. By contrast, another study found that strained In-O-In moieties can give rise to hole traps and that In-O-In, In-[OH]-In and In-In yield electron traps if the In atoms have unsaturated bonds[160]. In-O-P bridges are generally believed not to lead to trap states[160,163], although an increased number of levels near the valence band edge has been observed[160]. This collection of results indicates that trap formation is highly dependent on the exact configuration of the oxidized species. Indeed, computations on ligand-passivated QD models found that hole traps are formed by PO_2 moieties, but not by PO_3 and PO_4 (ref. 86). The effect of polyphosphates remained uncertain owing to their unclear oxidation state (leading to n-doping of the QDs) and to the large number of possible surface reconstructions. In addition, an investigation of the effect of various metal oxide shells around InP QDs found evidence for localized defect-like states near their surface in InP/InO, InP/GaO and InP/AlO core–shell systems but not in InP/CdO and InP/ZnO[166]. Although these results do not cover the entire range of possible oxidated species, they do show that oxidation does not necessarily have detrimental effects, which may explain the seemingly contradictory reports on the effects of InP oxidation.

Nevertheless, it is possible to prepare oxide-free InP QDs either under strictly anhydrous and oxygen-free reaction conditions or by using a hydrogen atmosphere[96,97]. Post-synthetic treatments can also remove oxidative defects. A popular post-synthetic treatment is etching with hydrogen fluoride (HF) (Fig. 3, 5 and 6). HF etching was used to clean and expose the surface of InP thin films as early as the 1960s[167] and was later shown to produce a completely oxide-free InP surface that was unachievable with other etching agents[168]. The first report of HF treatment to InP QDs observed a post-treatment increase in luminescence, which was attributed to fluoride ions filling phosphorus vacancies on the surface and replacing oxygen in the oxide layer[134]. Since then, different mechanisms have been proposed for trap passivation by HF. One possible mechanism for the increased luminescence after HF treatment under illumination is through removal of the phosphor as PF_3, leaving an indium-rich surface that could be better passivated by ligands[169,170]; elimination of phosphorous dangling bonds by fluoride was also supported by transient absorption results[139]. Alternatively, the increased quantum yield has been ascribed to the passivation of indium dangling bonds. This explanation is supported by observations that after HF treatment, carboxylate ligands exchange for fluoride ions and indium (oxo)hydroxides on the nanocrystal surface are removed[171]. Other studies have suggested that HF removes oxygen as PO_x species, rather than as indium hydroxides[74,172]. Recently, it was found that anhydrous HF reacts with InP to form InF_3 (a *z*-type ligand) and PH_3 and breaks up polyphosphate species into smaller PO_4 and PO_3 units. Although removal of polyphosphates was correlated with a higher luminescence efficiency, PO_4 and PO_3 species remained present on the surface of highly luminescent HF-treated samples, indicating that only some oxidized species form traps[86]. Given these varied results, it remains an open question as to which types of oxides can be removed by HF treatment, and in what ways their removal affects the optical

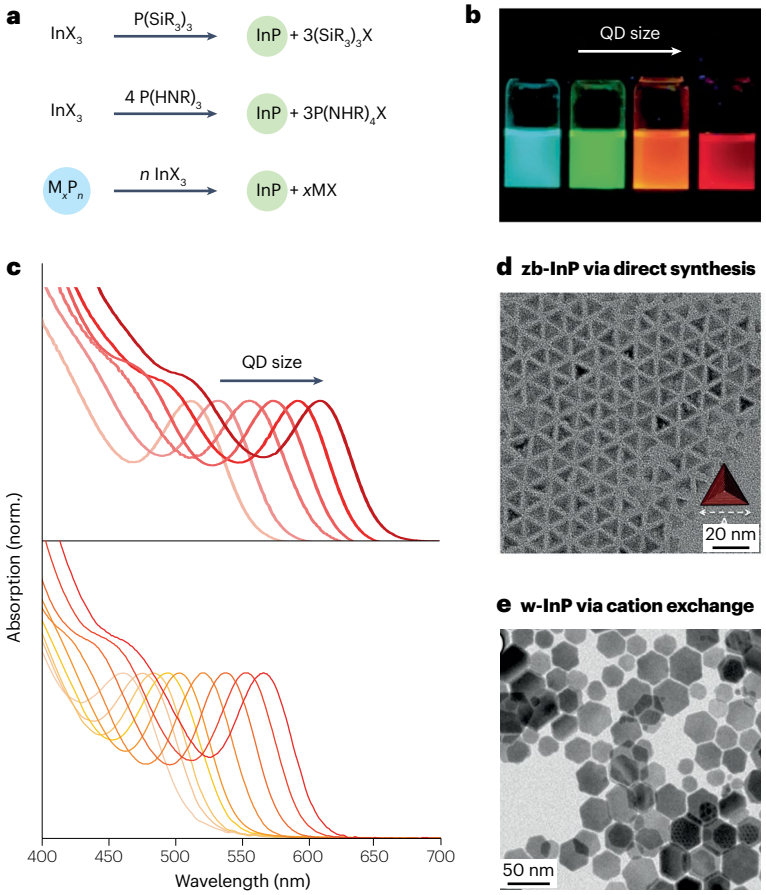

Fig. 2 | Synthesis and structure of InP quantum dots. a, InP quantum dots (QDs) can be prepared by reacting an InX_3 salt (in which X is a generic monovalent anion such as Cl^-, RCO_2^-, etc.) with (top) an organic silyl phosphine $P(SiR_3)_3$ or with (middle) an aminophosphine $P(HNR)_3$ in the presence of a reducing agent (such as the aminophosphine itself). Alternatively, InP QDs can also be prepared by transforming (cation exchanging) other metal phosphide nanocrystals into InP QDs (bottom). **b**,**c**, Photograph (under UV light) of samples prepared within our group (panel **b**) and absorption spectra of monodisperse InP QDs with band gaps spanning the visible range prepared using silyl phosphines (panel **c**). **d**,**e**, Electron micrographs of zinc-blende InP QDs with tetrahedral shape (panel **d**) and of wurtzite InP QDs in the form of platelets (panel **e**). Panel **b** image courtesy of L. van der Poll. Panel **c** adapted from ref. 74, Springer Nature Limited, and with permission from ref. 90, copyright 2021 American Chemical Society. Panel **d** reprinted with permission from ref. 77, Wiley. Panel **e** reprinted with permission from ref. 123, ACS.

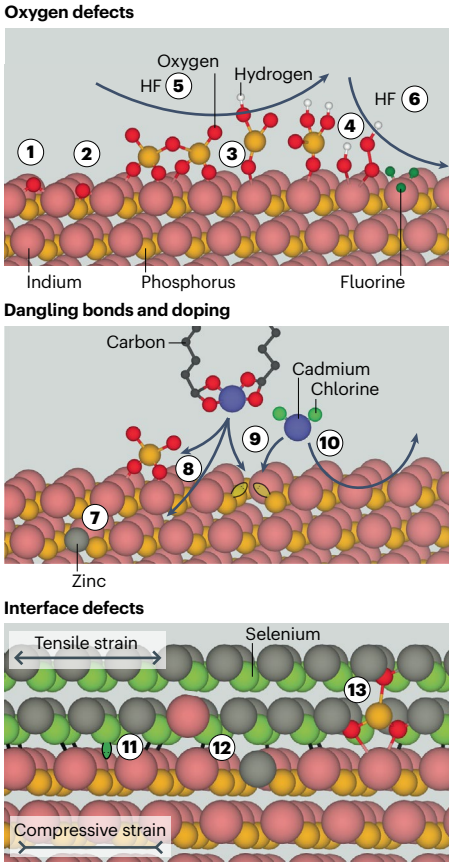

Fig. 3 | Documented structural defects in InP quantum dots and possible repair mechanisms. Oxygen defects include (1) In-O-In moieties[142,143,160], (2) In-O-P moieties[142,143,145,146,160,163], (3) PO_x moieties[85,86,135,136,138,143,145,150,151] and (4) In-OH and In-OOH moieties[149,160,171]. Several mechanisms have been proposed for the passivation of oxygen defects using hydrogen fluoride (HF) including (5) the breakage of PO_x into smaller PO_3 and PO_4 units[86] or (6) the replacement of In-bound hydroxide groups by fluoride anions[171]. (7) Lattice doping[79,137,179,195,197–201,203,204,208] and (8) incorporation of Cd in surface and subsurface[179]. (9) Dangling phosphorus bonds can be healed via z-type passivation[38,86,175–178] but (10) *z*-type exchange is also possible[152,174]. In core–shell structures, (11) strain-induced interfacial defects[197,232–234,236–238], (12) mixed interfaces[204,211,213,214,217,371] and (13) interfacial oxides[85,135,154] may also occur.

properties of nanoscale InP. HF treatment does have downsides: InP itself can be etched, causing unwanted spectral changes, and there are inherent dangers associated with using HF.

Because HF is hazardous, alternative fluorination strategies have also been proposed. Adding fluoride-rich ionic liquids either during the synthesis under microwave illumination, or post-synthetically, can strongly improve the quantum yield of the particles[173,174]. This effect has been ascribed to the passivation of electron traps when fluoride binds dangling indium bonds.

Surface states and *z*-type passivation

The main suspect for trap states in QDs has always been dangling bonds — that is, under-coordinated atoms at the surface of nanocrystals. Early theoretical calculations[175], later corroborated experimentally[176], predicted the existence of both electron and hole traps on the surface of InP QDs as a result of In and P dangling bonds, respectively. The traps appear to become 'deeper' as the QD size is reduced, owing to the shift of the band edges. Additionally, it has been shown that the formation of trap states owing to undercoordinated surface atoms depends on the shape of the QD[38]. In this work, cuboctahedral and In(111)-terminated tetrahedral models were deprived of a surface-capping moiety to simulate undercoordinated surface atoms. For cuboctahedrons, surface reconstruction prevents, in most cases, the formation of hole and electron traps. However, tetrahedral-shaped models are prone to form localized trap states within the band gap, resulting from undercoordinated In and P atoms.

Surface anions can be passivated by treating the particles with metal salts, also known as *z*-type ligands[152,174,177–179] (Fig. 3, 9). Treatment of InP with various *z*-type ligands has been shown to increase quantum yield (to 19% for Zn carboxylates and 49% for Cd oleate[177] or 11% for $CdCl_2$ (ref. 178)), which has been attributed to the passivation of dangling phosphor bonds. However, there is also evidence that cadmium carboxylate *z*-type ligands can bind both to phosphor and to phosphate present on the (sub)surface of InP nanoparticles [179] (Fig. 3, 8). More recently, it was shown that simple *z*-type passivation with InF_3 can increase quantum yields to 50–80% if the QDs are free of oxidized phosphorus species, specifically polyphosphates[35,86]. In addition, it was also observed that Cd^{2+} or Zn^{2+} can also replace surface In^{3+} ions (*z*-type exchange, Fig. 3, 10), relieving steric pressure on the surface and allowing for a more complete passivation, thus reducing trap states[174]. This exchange mechanism was supported by isothermal titration calorimetry experiments monitoring the treatment of InP with metal halides[152]. These results suggest that the *z*-type passivation mechanism may be more involved than previously thought.

Surface reconstructions may also have an important role in the creation or removal of surface states. In bulk solid state physics, it is well known that surfaces directly obtained from cleaving the bulk material are often not stable and will reconstruct[180]. For example, studies on GaAs surfaces have shown that the Ga-terminated (111) facet will reconstruct by creating Ga vacancies[181]. As-terminated (−1−1−1) facets are more complicated, and different reconstructions based on vacancies[182] or As-trimers have been proposed[183]. Although these reconstructions are relatively well understood for bulk surfaces, it is currently unclear whether they also take place on the QD surface. One study on CdSe QDs has shown that surface vacancies are necessary for the delocalization of the highest occupied molecular orbital and lowest unoccupied molecular orbital levels[184], highlighting the need for further studies on QD surfaces.

Doping

Impurities have long been incorporated into III–V semiconductors for doping purposes[185]. The incorporation of cations (other than group III) into InP QDs, however, has been pursued for two main reasons: optical doping (that is, Stokes-shifted emission) or linewidth narrowing. For instance, doping with Eu^{3+} yields multiple emission lines around the red spectral region[186]. Doping with Cu^{+} yields a broad emission in the NIR-I window (with photoluminescence efficiencies up to 80%), ascribed to hole localization and to structural relaxation around the Cu site[187–194].

Zn^{2+} ions are commonly introduced as additives during the synthesis of InP QDs to obtain QDs with narrower (ensemble) linewidths[195–197]. However, aliovalent impurities such as Zn^{2+} are known dopants for III–V semiconductors[198–202] and appear to diffuse and be incorporated into InP QDs[179,203] (as illustrated in Fig. 3, 7). Various spectroscopic analyses

have concluded that the incorporation of Zn introduces shallow hole states and associated lattice disorder[200]. Moreover, other results suggest that the incorporation of Zn in the InP core limits the performance of core–shell structures[137,204]. Nevertheless, photoluminescence quantum yields of approximately 90% have been reported for both InP and In(Zn)P[79,137,159,205–208] QDs shelled with $ZnSe_{1-x}S_x$ (where In(Zn)P = InP QDs incorporating Zn in the InP lattice).

Several questions about doping remain open, including what lattice positions the extrinsic ions occupy, whether electronic doping occurs or whether there are doping compensation mechanisms also at play.

Heterovalent core–shell interfaces

Epitaxial growth of II–VI on III–V semiconductors (including InP QDs) has been extensively investigated. The heterovalent nature of such interfaces introduces complexity, and it is worthy to highlight insights from works on lattice-matched GaAs/ZnSe (001) polar junctions. First, we note the efforts to reduce the density of stacking faults in the ZnSe overlayers[209,210]. Second, computational studies have shown that an abrupt interface is thermodynamically unstable and that a mixed and/or a defected interface is energetically favoured[211,212] (Fig. 3, 12), and experiments also support the existence of mixed and defected interfaces in samples with a low density of stacking faults[213]. Furthermore, the composition of stable mixed interfaces is known to be orientation-dependent[214].

Coating InP QDs with $ZnSe_{1-x}S_x$ shells enables highly efficient and stable emitters. These III–V/II–VI core–shell systems must have a balanced stoichiometry[137,204,215,216]. In particular, results strongly suggest that a InP/(In,Zn)P/ZnSe interface boosts the photoluminescence efficiency of InP/$ZnSe_{1-x}S_x$ QDs beyond 90%[204,217], and that a selenium-terminated interface might be important to limit the diffusion of zinc[218,219] and sulfur[137,216] into the InP cores. Interfaces containing oxidized species have also shown to improve the performance of InP QDs[154,220] (Fig. 3, 13).

Strain

In core–shell QDs, strain can arise from the lattice mismatch between core and shell materials, causing several consequences[221]. It can introduce (strain-relieving) defects[222] (Fig. 3, 11), alter band offsets[223,224], shift vibrational frequencies[225], give rise to piezoelectric fields[226] or even impact the fine structure[227–229], electron–phonon coupling[230] and photon out-coupling[231].

However, little is known about strain engineering in InP QDs. In bulk InP, a phase transition (to rock salt) closely followed by a direct-to-indirect transition (as the X band crosses under Γ) occurs at lattice contractions of about 3–5% (approximately 10 GPa)[232,233], and similar values are found for InP QDs[234–236]. In InP/$Zn_{1-x}Cd_xSe$ core–shell systems, strain can be tuned from compressive (InP/ZnSe) to tensile (InP/CdSe) with no strain observed at x approximately 0.4 (ref. 237). Computations suggest that even a thin ZnSe shell can build considerable tensile strain and could lead to a considerable energy shift of the highest occupied molecular orbital[197]. More pronounced effects are found with ZnS shells, which could be related to not only its smaller lattice constant but also its larger Young modulus[238] (see Table 1 for mechanical properties). These computational results also point to a decrease in band gap with increasing tensile strain. However, experiments have shown the opposite trend — a considerable increase in band gap with increasing strain — that could be of potential interest for piezochromic applications[234,236].

Wavefunction engineering

Control over the energy landscape is fundamental in QD technologies[13,14]. Although tuning the surface ligands might achieve this control to a limited extent[171,239], shape-control and core–shell structuring are more versatile and robust avenues of control. Core–shell structuring, in particular, has been pivotal to the development of performant and stable QDs. For instance, in type I heterostructures, both the electron and hole wavefunctions are confined to the core, which allows undesirable surface states and reactions to be avoided. In type II heterostructures, the electron and hole wavefunctions are spatially separated, which allows the radiative lifetimes to be increased and the band gap to be reduced. We note that band offset is one of the key parameters in the classification and design of semiconductor heterostructures (Fig. 4a,b). However, determining the band offsets in QD heterostructures is not straightforward because the degree of quantum confinement needs to be taken into account, as well as any interface dipoles[240]. The latter is particularly relevant to heterovalent systems such as InP/$ZnSe_{1-x}S_x$ core–shell structures[241].

Type I InP/$ZnSe_{1-x}S_x$ core–shell structures

Type I InP/$ZnSe_{1-x}S_x$ core–shell QDs have been widely studied and implemented in commercial products. ZnSe and ZnS exhibit complementary properties for shelling InP. On the one hand, ZnSe has a small lattice mismatch to InP (3.4%) but does not provide a robust type I confinement, especially for smaller InP cores. On the other hand, ZnS ensures a robust type I band alignment (regardless of core size) but has a large lattice mismatch (7.8%), which appears to broaden the emission of the QDs[242]. Finding a balance between the size of the InP core and the composition and structure of the $ZnSe_{1-x}S_x$ shell can overcome these limitations and obtain highly efficient narrow band emitters (Fig. 4c,d). For instance, red-emitting InP/ZnSe/ZnS core–shell–shell structures with near-unity photoluminescence efficiency and linewidths of 110–130 meV have been realized (including non-blinking QDs)[74,137,172], as have green-emitting InP/$ZnSe_{1-x}S_x$/ZnS ($0.5 < x < 0.67$) heterostructures with efficiencies around 90% and slightly broader linewidths (160–210 meV)[79,205,206,242]. Blue-emitting systems are, so far, least performant with efficiencies and linewidths of 45% and 260 meV, respectively[207,243]. It is not yet clear why green-emitting and blue-emitting QDs have lower performance than red, but it could be related to interfacial defects and strain induced by the increased lattice mismatch of the shell and to the fact that strain is more problematic for smaller structures as they are less able to relax strain within the material[238]. Interfacial strain can be relieved by alloying the $ZnSe_{1-x}S_x$ shell with other divalent cations[237,244]. In addition, the efficiency of green and blue emitters could be limited by defects in the shell (stacking faults, impurities and so on)[217,245–251]. The broader linewidths likely arise from a combination of synthetic and intrinsic drawbacks inherent to the extremely small sizes of the InP cores (such as size distribution requirements and increased homogeneous linewidths), but can be made more narrow by Zn doping of the cores. Blue-emitting and green-emitting In(Zn)P/$ZnSe_{1-x}S_x$ core–shell QDs with improved quantum yields and narrower linewidths have been demonstrated, although their structures remain unclear and might be quite complex[79,137,159,205–208].

Despite their generally high efficiencies and stabilities, these QDs have room for improvement. For instance, the relatively thick $ZnSe_{1-x}S_x$ shells make the QDs less compact, which can undermine phosphor and lasing applications. Another perhaps more pressing limitation is their relatively short bi-exciton lifetimes, preventing efficient operation at high exciton density[74]. For instance, highly efficient red-emitting

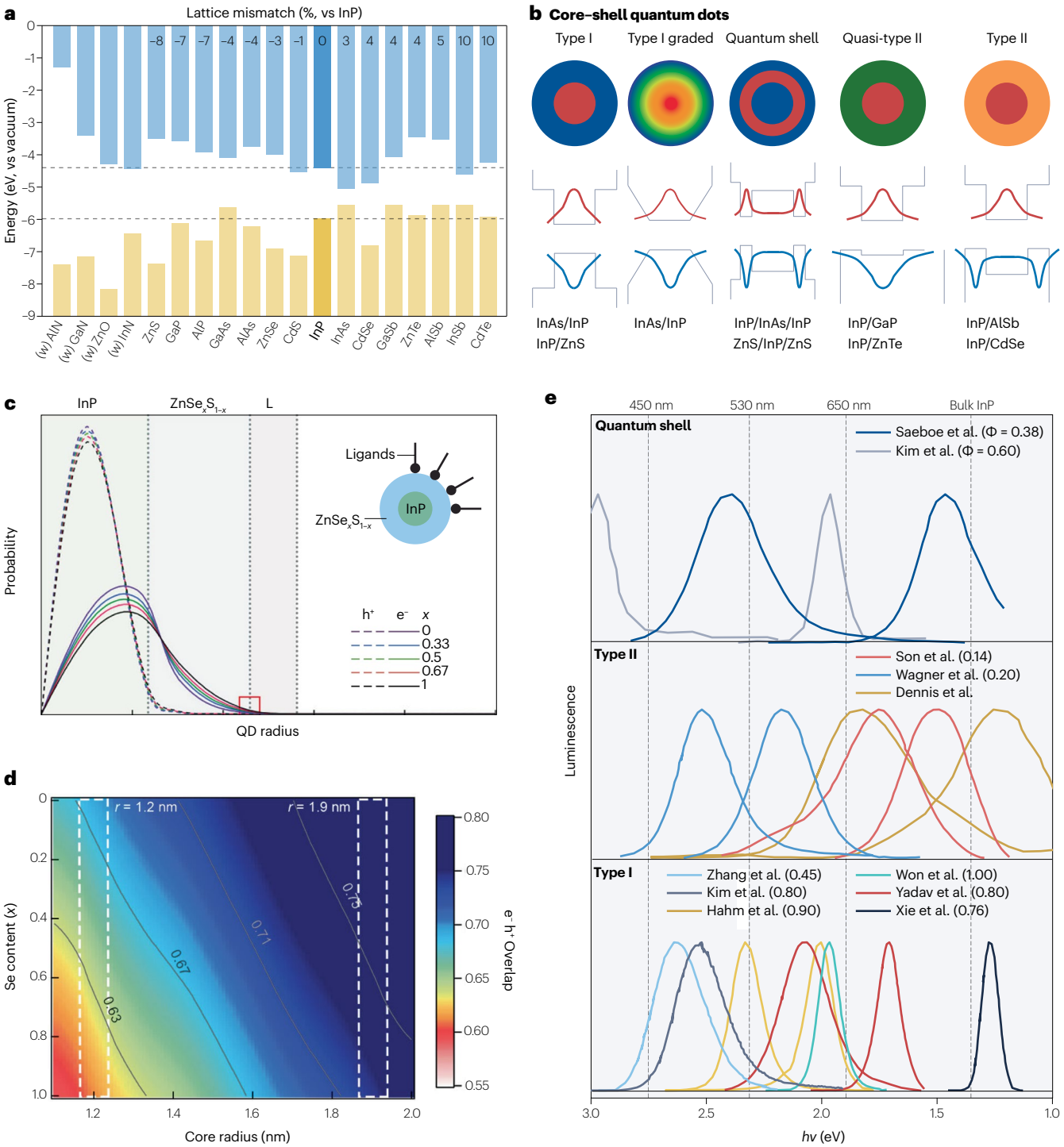

Fig. 4 | InP-based core–shell quantum dots. a,**b**, The band offsets of bulk semiconductors[366,372] (panel **a**) are usually used as a first approximation in the design of core–shell quantum dot (QD) structures (panel **b**), which can be classified into various types according to the (de)localization of electron and hole wavefunctions (the electron and hole probability distribution functions are depicted in red and blue, respectively). **c**,**d**, In fact, quantum confinement also has an important role in the design, and in InP the conduction levels are thought to be more sensitive to it than the valence levels. For instance, type I confinement in InP/$ZnSe_xS_{1-x}$ QDs is achieved by using shells with a large sulfur content (panel **c**) and/or by using larger cores (panel **d**). **e**, Photoluminescence spectra of selected InP-based core–shell structures emitting in the visible or near infrared, reported efficiencies Φ in parenthesis. Panels **c** and **d** adapted with permission from ref. 242. Copyright 2019 American Chemical Society. Data in panel **e** are from Saeboe et al.[284], Kim et al.[285], Son et al.[300], Wegner et al.[269], Dennis et al.[297], Zhang et al.[243], Kim et al.[270], Hahm et al.[242], Won et al.[74], Yadav et al.[93] and Xie et al.[275].

InP/ZnSe/ZnS core–shell–shell QDs exhibit exciton lifetimes of 13 ns but bi-exciton lifetimes of only 50 ps (ref. 74). In this system, the negative trion is rather long-lived (5.3 ns), owing to the delocalization of the electron wavefunction into the thick ZnSe shell (3.5 nm)[252], suggesting that the short bi-exciton lifetime results from a sharp hole confinement. Smoothing the confinement potential using compositionally graded core–shell QDs might be an effective approach to mitigate this, as it has found enormous success in II–VI QDs. Graded $ZnSe_{1-x}S_x$ shells grown on InP QDs have not only extended the negative trion lifetimes by approximately four times but also reduced luminescence intermittency (blinking) and spectral diffusion as the grey state appears to originate from the negative trion itself[79,253,254]. These types of shells should improve the performance and stability of quantum LED (QLEDs) as excess electrons often accumulate in the QD layer owing to the imbalanced charge injection rates; however, they do not fix the sharp hole confinement at the core–shell interface and therefore are unlikely to increase bi-exciton lifetimes.

The fact that long bi-exciton lifetimes remain elusive raises the question as to whether these types of shells can promote efficient optical gain. The development of gain in InP/ZnSe QDs has been thoroughly studied by transient absorption spectroscopy[255]. This analysis indicated that, at room temperature, gain can be understood as originating from state filling of the lowest electron level with a degeneracy of 2 and of the lowest hole level with an effective degeneracy of 5–10. This effective hole degeneracy is higher than the expected degeneracy of 4, which was attributed to the thermal population of higher states in the valence band, perhaps arising from the ZnSe shell. In addition, it was also observed that optical gain was limited to about 10% of the theoretical maximum value, owing to a loss of charge carriers at high exciton density attributed to hole trapping. Hole trapping in this system has also been studied in other works and has been ascribed to In atoms in the ZnSe shell[248,256].

Quest for all-III–V type I core–shell structures

In principle, shelling InP with a III–V semiconductor should enable QDs with dipole-free interfaces and the graded core–shell structures needed to mitigate Auger-related losses[257–262]. In fact, lasing quality has been demonstrated using vapour-phase grown InP QDs encapsulated by $Al_xGa_yIn_zP$ layers[263]. However, InP QDs with III–V shells remain rather unexplored for a number of reasons. First, the two evident shelling materials, $In_{1-x}Ga_xP$ and $In_{1-x}Al_xP$, are characterized by direct-to-indirect crossovers at $x = 0.8$ and 0.4, respectively, which complicates the prediction of band offsets. Furthermore, it is not clear whether these materials can effectively provide a type I confinement to InP QDs[264–267]. Second, owing to their indirect nature, GaP and AlP shells would strongly reduce the absorption cross-section of the QDs. Third, similar to InP, these materials are prone to oxidation and many Ga precursors appear to react with InP QDs to form $In_{1-x}Ga_xP$ alloys, complicating the growth of core–shell structures[268–270]. The few reports on these structures have been limited to InP/GaP core–shells, mostly in combination with ZnS outer shells[269,271–273]. Mixed-anion alloys also remain unexplored but could be another avenue to access wide direct gap shelling materials with a type I band alignment. For example, vapour-phase grown InP/$GaAs_{0.6}P_{0.4}$ dot-in-a-well lasers have been demonstrated[274].

According to bulk band alignments, InP could also be envisaged as a (type I) shell material for infrared emitting InAs QDs. InAs/InP and $InP_{1-x}As_x$/InP core–shell QDs have been developed to emit in the range of 600–1,000 nm (refs. 118,275,276). Although their photoluminescence efficiencies were initially quite low (<5%), subsequent shelling with ZnSe improved them substantially (to around 76%). Similarly, for multishell In(Zn)As/In(Zn)P/GaP/ZnS QDs emitting at approximately 800–1,000 nm (refs. 277,278), the photoluminescence efficiency of the In(Zn)As core (2.5%) increased to 33%, 46% and 75% with each successive shell.

Reverse core–shell–shell structures

Reverse core–shell–shell structures, also known as quantum shells, offer band-gap tunability and room for mitigating Auger losses[279–283]. In this configuration, an InP mid-shell is grown between a core and an outer shell of wider gaps, with the band gap determined by the core size and the shell thickness. For instance, systems such as ZnSe/InP/ZnS and CdTe/InP/ZnS QDs have been shown to exhibit tunable and efficient emission across the NIR-I[284–286]. However, these structures have not been much explored, and whether they can actually mitigate Auger processes remains an open question.

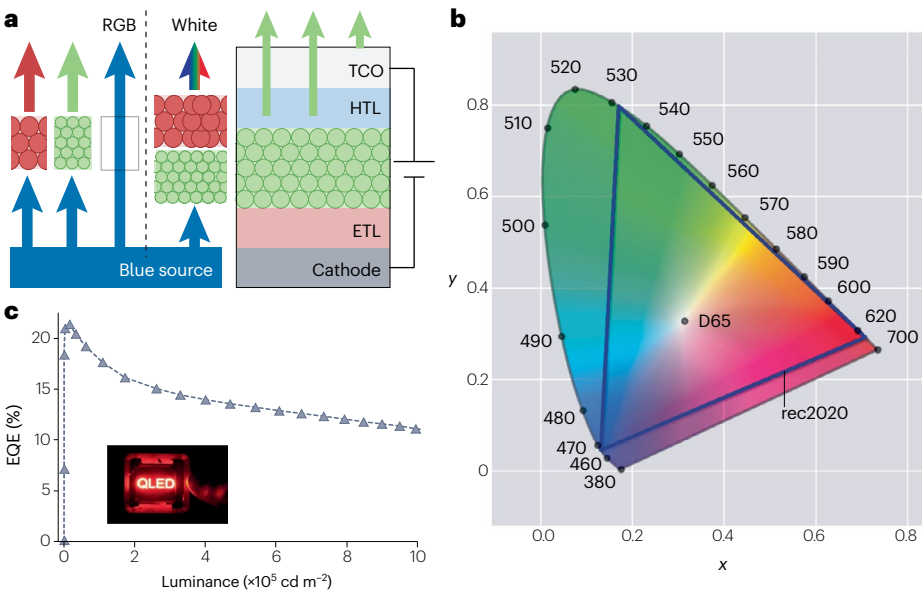

Fig. 5 | InP-based quantum dots in light-emitting diodes. In luminescent down-converting devices, quantum dots (QDs) convert blue photons into less energetic photons (such as green or red), whereas in electroluminescent devices QDs convert electrical energy into photons (panel **a**). The high colour purity of red InP and green In(Zn)P light-emitting diodes (LEDs) is already in close agreement with the requirements for a wide colour space of rec2020 standards (the tips of the triangle are the coordinates of highly pure red, green and red, and D65 represents the coordinates for white light) (panel **b**). At low powers, QDs with near-unity photoluminescence efficiencies have been successfully implemented in efficient LEDs. However, at high powers, the efficiency droop remains a problem. This can be clearly seen in the external quantum efficiency of an electroluminescent InP-based quantum LED (QLED) as a function of brightness (panel **c**). EQE, external quantum efficency; ETL, electron transporting layer; HTL, hole transporting layer; RGB, red, green and blue; TCO, transparent conducting oxide. Panel **c** adapted from ref. 74, Springer Nature Limited.

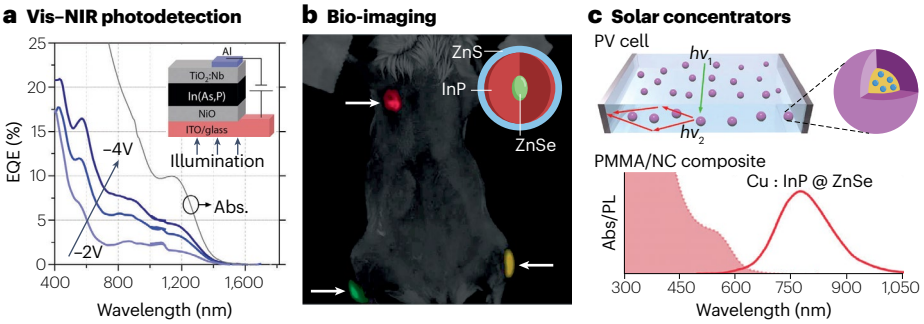

Fig. 6 | Near-infrared applications of InP quantum dots. a, Photodetectors with high external quantum efficiency (EQE). **b**, Bio-imaging. In this photograph, quantum dots are used to probe different parts of a mouse. **c**, Solar concentrators. With a large Stokes shift, Cu:doped InP quantum dots down-convert visible photons to infrared photons, which are then guided by a waveguide, such as a polymethyl methacrylate (PMMA) matrix, to solar panels placed on the side. NC, nanocrystal; NIR, near-infrared; PV, photovoltaic. Panel **a** adapted from ref. 344, CC BY 4.0. Panel **b** adapted with permission from ref. 284. Copyright 2021 American Chemical Society. Panel **c** adapted with permission from ref. 191, Elsevier.

Type II and quasi-type II structures

Type II and quasi-type II structures allow for spatial delocalization and separation of electrons and holes within the dot, which, in turn, reduces the band gap and increases the Stokes shift as well as the carrier lifetimes[287–289]. These structures have found interest for photovoltaic and photo-electrochemical cells[290–292], photocatalysis[293], down-converters for solar concentrators[294] and also gain medium[295,296]. For example, in NIR-emitting InP/CdS core–shell QDs, both the exciton and bi-exciton lifetimes increased with increasing shell thickness, with values up to 702 ns and 7 ns, respectively[297]. The charge transfer rate to methylviologen[298] and the multiple exciton generation quantum yield[299] are also not affected by the quasi-type II band alignment, making these QDs interesting for QD-based solar cells. Cd-free alternatives expand their potential to biological applications. For instance, InP/ZnTe/ZnSeS QDs emitting in the NIR have been realized with exciton lifetimes of 387 ns (ref. 300). InP/ZnO QDs have also been proposed for LEDs[158,301], solar concentrators[155] and artificial retinas[302], although the exciton lifetimes in these structures appear to be shorter, around 31 ns. The luminescence efficiency of type II QDs can be limited by surface traps, but in principle this can be mitigated by efficient surface passivation or by growing an outer type I shell[158,303].

InP QDs in photonic technologies

RGB phosphors

Cyan, green and red QDs with bright, narrow and stable emission are strong contenders for optical down-conversion in display and lightning technologies. Down-converting blue light into red or green through a QD film is a simple and efficient way to upgrade a blue LED array into a full colour display (Fig. 5a). Converting blue into both red and green light is also appealing for constructing white emitting diodes using a single blue source (Fig. 5a), and it circumvents both the poor efficiency of green as well as the high cost of red in the three-diode approach to white light generation. In addition, the tunability of QD phosphors enables customized spectral outputs.

For QDs to be used as down-converters in high-intensity applications such as LED lamps, they require strong blue absorptivity, narrow emission line (colour purity), near-unity quantum yield and stability at high photon fluxes (no droop) and at elevated temperatures. Such properties have been obtained for Cd-based type I QDs[304], but droop remains a major challenge in InP-based dots[250]. Various design strategies can mitigate Auger recombination in InP QDs, such as trap passivation[139] and incorporation of a thick mid-shell[38] or graded shell[254]. In the latter approach, negative trion Auger recombination can be strongly reduced through potential smoothing in gradient shells, but extended bi-exciton lifetimes remain elusive in these systems. Furthermore, the brightness of InP QDs is limited by the relatively weak blue absorptivity of thick $ZnSe_{1-x}S_x$ shells, so innovative shell engineering solutions such as using more compact shells[305] or alternative materials[306] may be required. Smaller InP QDs also exhibit wider linewidths and lower efficiencies, although incorporating Zn into the cores overcomes these limitations[205].

Commercial use of InP QDs as blue-down-converters in display and lighting technology seems close on the horizon. Red InP QDs have already been shown to be a viable on-chip solution for use in white LEDs using traditional green-yellow phosphors[307]. White LEDs composed fully of InP QDs were also achieved in an early demonstration by avoiding Förster resonance energy transfer processes between QDs of different colours (sizes), in this case red and green[308]. Furthermore, InP QDs are being integrated into up-and-coming μLED displays[17,309]. Finally, InP QDs may be a solution to the growing interest in cyan phosphors for healthy lighting[310–314] and may be of interest for specialty applications such as custom illumination (for example, indoors or in horticulture), green-house roofs, security inks and so on.

Electroluminescent QLEDs

Theoretically, electroluminescence is a more efficient way to obtain light from QDs compared with down conversion, and there have been many attempts to construct InP QD-based LED devices to this end[17,29,74,137,315–322] (Fig. 5a). Electroluminescent QLEDs are particularly appealing for display applications, because the high colour purity of red InP and green In(Zn)P QLEDs already closely agrees with the requirements for a wide colour space of rec2020 standards[28] (Fig. 5b).

Currently, record efficiencies stand at 22.2% for red[172], 16.3% for green[323] and 2.8% for blue[324,325] devices. To construct highly efficient LEDs, device structure and materials must be carefully chosen to ensure exciton confinement inside the QDs to prevent parasitic or trap emission in the device (this can be achieved by growing a thick type I shell around the InP cores)[318] and balanced electron and hole injection currents. Compared with II–IV materials, the high-lying valence band edge of InP QDs makes electron (hole) injection comparatively hard (easy)[318]. Despite the impressive near-limit efficiencies reached in red InP/$ZnSe_{1-x}S_x$ QLEDs, the efficiency droop at higher operation power and the lifetime still need to be improved (Fig. 5c).

Into the infrared

Light sources in the far-red and NIR range are increasingly required for applications in biology and medicine[326–330], computer vision[331] and

data transmission at both short and long (fibre) ranges[263,332–334]. Infrared QDs in this range[335,336], owing to their small size, tunable surface chemistry and processing versatility, extend the application window of these light sources to miniaturized devices such as µLEDs or photonic chips[17,25], nano-imaging[337], fluorescent (bio) markers[338], optical sensors, security inks and so on. In addition, infrared QDs with high absorption cross-sections and carrier mobilities are of great interest for infrared detection and imaging technologies[339] and for photovoltaics[340].

In spite of a bulk band gap of 1.35 eV, and most research being conducted on green and red sizes, InP is still in the competition for far-red to short-wave infrared (<1 eV) applications. Although the synthesis of large-sized InP QDs remains challenging, InP structures emitting in this range have been reported, namely, wurtzite QDs[125], reverse heterostructures, $InP_{1-x}As_x$ alloys[118,121], doped QDs and InAs-InP core–shell QDs, together with early demonstrations of in vivo imaging[118,284,341], solar cells[342,343], LEDs[277,278] and photodetectors[344] (Fig. 6). In addition, InP QDs have been used in efficient (photon) up-converting systems[345]. Large-sized InP QDs are expected to have higher absorption cross-sections, narrower linewidths, longer bi-exciton lifetimes and higher film mobilities (although still limited to <0.5 $cm^2 V^{-1} s^{-1}$)[128] compared with their smaller counterparts – appealing characteristics that continue to motivate their development.

Broadband infrared sources based on InP QDs can also be envisaged, either by combining InP QDs emitting at various wavelengths (as in the case of the white LED) or by doping InP with elements such as Cu. Cu^+ doping results in an efficient, broad emission that is spectrally tunable with doping concentration[187,192]. Given their large Stokes shift, Cu-doped InP QDs have also raised interest for luminescent solar concentrators[155,191] (Fig. 6c).

Coherent and quantum light

QDs are promising active materials for optical amplifiers, super luminescent diodes and lasers[19]. Optical gain and lasing from QDs have been intensely studied over the past two decades[19,346], and the development of gain in CdSe is now well understood[347]. Although the physics of gain in InP is expected to be similar to that of CdSe given their similar electronic structures, it remains much less studied in InP QDs. Gain, amplified spontaneous emission and lasing have been observed in InP/$ZnSe_{1-x}S_x$ QDs (Fig. 7a–c), but loss processes such as trapping and Auger recombination severely limit gain. In addition, the effective (band edge) degeneracies in InP/$ZnSe_{1-x}S_x$ QDs remain far from understood[255,348].

Highly efficient InP-based QDs with robust optical performance in the multi-exciton regime and with well-controlled degeneracies are yet to achieved. Further studies on size and shape effects, and on

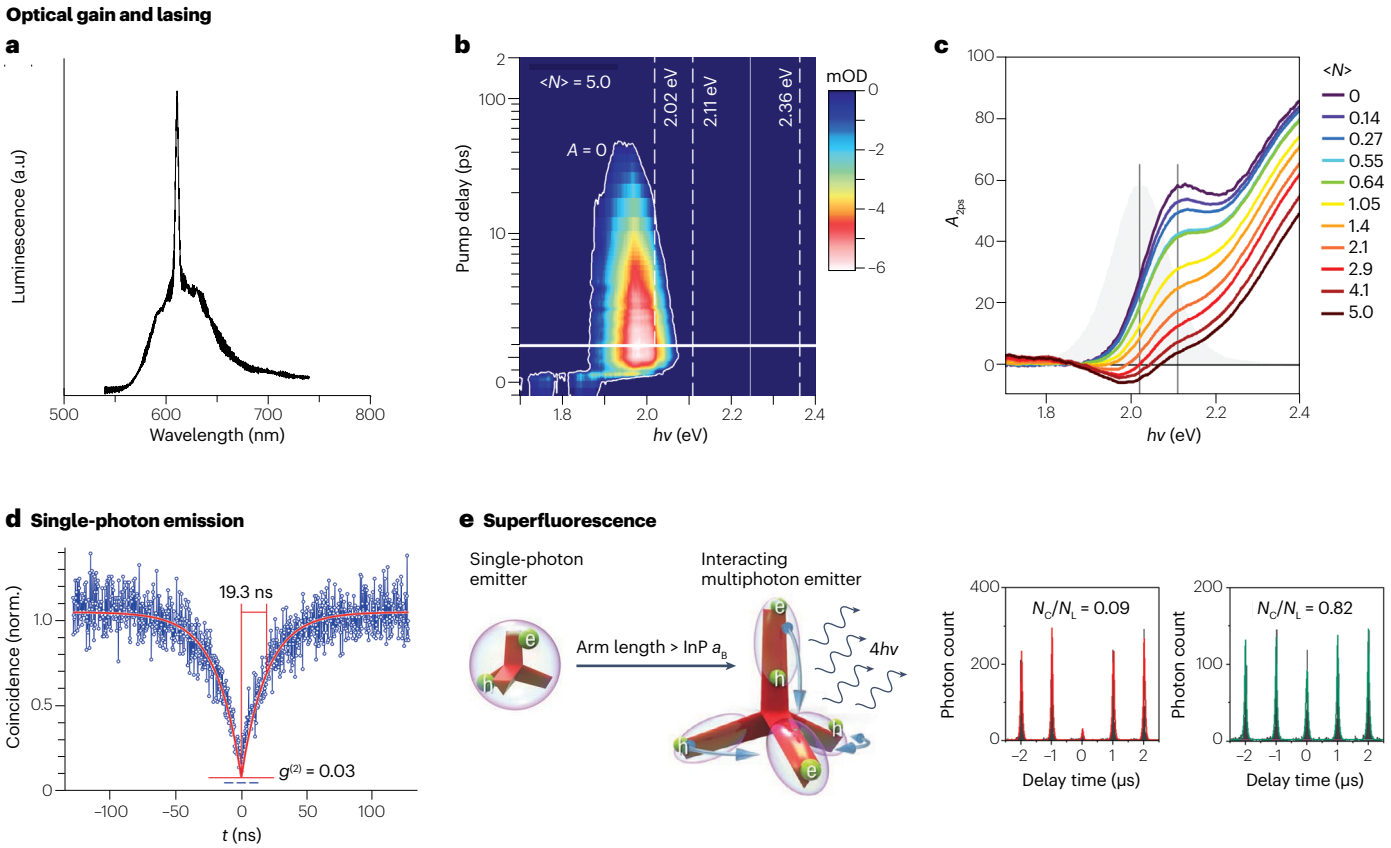

Fig. 7 | Coherent and quantum light sources using InP quantum dots. a, Lasing using InP quantum dots has been demonstrated. **b**,**c**, However, ultrafast transient absorption spectroscopy reveals that the multi-excitons remain relatively short-lived (panel **b**) and that optical gain is also rather weak (<*N*> denotes the average number of excitons per dot and A_{2ps} is the absorption at a pump–probe delay of 2 ps) (panel **c**). **d**, Highly pure (incoherent) single-photon emission has also been demonstrated under continuous-wave excitation. **e**, Single InP tetrapods with long arms can emit multiphotons coherently, that is, in a superfluorescent fashion. a.u., arbitrary unit; mOD, optical density, milli. Panel **a** adapted with permission from ref. 348, © The Optical Society. Panels **b** and **c** adapted with permission from ref. 255, Wiley. Panel **d** adapted with permission from ref. 361. Copyright 2017 American Chemical Society. Panel **e** adapted with permission from ref. 364, Wiley.

compositionally graded and strain-engineered heterostructures, might address this gap[227–229,257–262]. Alternatively, type II structures allowing for single-exciton gain could be envisaged[295].

QDs are also promising emitters for single-photon and entangled-photon sources[23,334,349,350]. For efficient generation of undistinguishable single photons, the optical coherence time needs to approach twice the spontaneous emission lifetime. The generation of entangled photon pairs, instead, can be achieved through the bi-exciton–exciton cascade[350–353], known to occur in InAs QDs[354,355]. The development of such light sources using InP QDs is an outstanding challenge, with only few studies observing fast dephasing ascribed to phonons[356–360], and will require not only improved QD design but also optimized device architectures and efficient fabrication methods. Nevertheless, high-purity single-photon emission was observed in InP/ZnSe QDs under intense continuous-wave pumping (Fig. 7d), owing to the combination of efficient luminescence and efficient Auger recombination of multi-excitons. This result highlights the potential of these systems for on-demand (incoherent) single-photon sources operating at room temperature[361].

Finally, super luminescence from QD arrays is an emerging subject of research[362,363]. Although InP QD arrays, specifically, have not been investigated in this regard, super luminescence was observed from a single tetrapod-shaped InP QD with long arms and ascribed to excitons in different arms interacting through quantum tunnelling[364] (Fig. 7e).

Outlook

The quality of InP QDs has improved considerably, especially over the past decade. Today, InP QDs emitting in the visible are manufactured at industrial scale for the LED market. However, many aspects of their quality still lag behind those of II–VI or halide perovskite QDs and do not meet expectations for applications, including LEDs. In other words, their current commercial appeal still primarily lies in their compliance, in terms of elemental composition, with regulations on consumer electronics. Improving the quality of InP-based QDs is therefore key to making them more competitive in the technological market. This requires advances on multiple fronts.

First, fundamental understanding about the electronic structure of InP-based QDs remains scarce, which limits the design of these QDs for specific applications. In addition, their rich but often poorly controlled structure complicates understanding of their structure–property relationships and hence their applicability. Specifically, further investigations are required to understand how their size, shape, phase and composition affect the density of states, exciton fine structure, structural dynamics, electron–phonon coupling and related quantities such as the fundamental linewidths and coherence times, emission lifetimes, Auger recombination of multiple excitons, polarization of the emitted light and so on.

To fill this void, ambitious structure–property studies using state-of-the-art know-how will be required as well as new synthetic methods that produce InP QDs with desired size, shape, phase and composition (in the core, at surface, at the core–shell interface and also in terms of doping levels). Given the commercial interest of these QDs, safe, robust and scalable methods allowing the production of these QDs at full reaction yields and at reduced costs would also be highly valuable.

The surface of InP QDs also remains largely unexplored and can be engineered towards achieving high brightness, improved stability or highly conductive films. Other functionalities may also be incorporated by modifying the surface such as chirality (such as for polarization-selective photodetectors) or biological activity (such as for theranostics).

The library of core–shell structures must be expanded to surpass current limitations in terms of efficiency, linewidths, brightness, compactness, gain, coherence, stability (chemical, electrochemical, doping, thermal) and so on. So far, InP/$ZnSe_{1-x}S_x$ core–shell QDs have attracted the most popularity, but their performance and range remain limited. Nevertheless, a wide window of interesting opportunities remains rather unexplored, such as all-III–V QDs (including alloys).

Finally, applications beyond visible LEDs should be further explored and optimized. These applications include lasers, infrared technologies, photocatalysis, piezochromism, solution-processed electronics and others.

Published online: 12 October 2023

References

1. Dingle, R., Wiegmann, W. & Henry, C. H. Quantum states of confined carriers in very thin $Al_xGa_{1-x}As$-GaAs-$Al_xGa_{1-x}As$ heterostructures. *Phys. Rev. Lett.* **33**, 827–830 (1974).
2. Sakaki, H. Scattering suppression and high-mobility effect of size-quantized electrons in ultrafine semiconductor wire structures. *Jpn. J. Appl. Phys.* **19**, 735–738 (1980).
3. Ekimov, A. & Onushchenko, A. Quantum size effect in three-dimensional microscopic semiconductor crystals. *JETP Lett.* **34**, 345 (1981).
4. Efros, A. L. & Efros, A. L. Interband absorption of light in a semiconductor sphere. *Sov. Phys. Semicond.* **16**, 772–775 (1982).
5. Brus, L. E. A simple model for the ionization potential, electron affinity, and aqueous redox potentials of small semiconductor crystallites. *J. Chem. Phys.* **79**, 5566–5571 (1983).
6. Brus, L. E. Electron–electron and electron–hole interactions in small semiconductor crystallites: the size dependence of the lowest excited electronic state. *J. Chem. Phys.* **80**, 4403–4409 (1984).
7. Meyer, M., Wallberg, C., Kurihara, K. & Fendler, J. H. Photosensitized charge separation and hydrogen production in reversed micelle entrapped platinized colloidal cadmium sulphide. *J. Chem. Soc. Chem. Commun.* **2**, 90–91 (1984).
8. Murray, C. B., Norris, D. J. & Bawendi, M. G. Synthesis and characterization of nearly monodisperse CdE (E = sulfur, selenium, tellurium) semiconductor nanocrystallites. *J. Am. Chem. Soc.* **115**, 8706–8715 (1993).
9. Yin, Y. & Alivisatos, A. P. Colloidal nanocrystal synthesis and the organic–inorganic interface. *Nature* **437**, 664–670 (2005).
10. Calvin, J. J., Brewer, A. S. & Alivisatos, A. P. The role of organic ligand shell structures in colloidal nanocrystal synthesis. *Nat. Synth.* **1**, 127–137 (2022).
11. Kovalenko, M. V. et al. Prospects of nanoscience with nanocrystals. *ACS Nano* **9**, 1012–1057 (2015).
12. Efros, A. L. & Brus, L. E. Nanocrystal quantum dots: from discovery to modern development. *ACS Nano* **15**, 6192–6210 (2021).
13. Pietryga, J. M. et al. Spectroscopic and device aspects of nanocrystal quantum dots. *Chem. Rev.* **116**, 10513–10622 (2016).
14. García de Arquer, F. P. et al. Semiconductor quantum dots: technological progress and future challenges. *Science* **373**, eaaz8541 (2021).
15. Liu, M. et al. Colloidal quantum dot electronics. *Nat. Electron.* **4**, 548–558 (2021).
16. Rhee, S., Kim, K., Roh, J. & Kwak, J. Recent progress in high-luminance quantum dot light-emitting diodes. *Curr. Opt. Photon.* **4**, 161–173 (2020).
17. Liu, Z. et al. Micro-light-emitting diodes with quantum dots in display technology. *Light Sci. Appl.* **9**, 83 (2020).
18. Nannen, E., Frohleiks, J. & Gellner, S. Light-emitting electrochemical cells based on color-tunable inorganic colloidal quantum dots. *Adv. Funct. Mater.* **30**, 1907349 (2020).
19. Park, Y.-S., Roh, J., Diroll, B. T., Schaller, R. D. & Klimov, V. I. Colloidal quantum dot lasers. *Nat. Rev. Mater.* **6**, 382–401 (2021).
20. Jung, H., Ahn, N. & Klimov, V. I. Prospects and challenges of colloidal quantum dot laser diodes. *Nat. Photon.* **15**, 643–655 (2021).
21. Pejović, V. et al. Infrared colloidal quantum dot image sensors. *IEEE Trans. Electron. Devices* **69**, 2840–2850 (2022).
22. Nakotte, T. et al. Colloidal quantum dot based infrared detectors: extending to the mid-infrared and moving from the lab to the field. *J. Mater. Chem. C* **10**, 790–804 (2022).
23. Kagan, C. R., Bassett, L. C., Murray, C. B. & Thompson, S. M. Colloidal quantum dots as platforms for quantum information science. *Chem. Rev.* **121**, 3186–3233 (2021).
24. Chen, J. & Rong, K. Nanophotonic devices and circuits based on colloidal quantum dots. *Mater. Chem. Front.* **5**, 4502–4537 (2021).
25. Chen, M., Lu, L., Yu, H., Li, C. & Zhao, N. Integration of colloidal quantum dots with photonic structures for optoelectronic and optical devices. *Adv. Sci.* **8**, 2101560 (2021).
26. Click, S. M. & Rosenthal, S. J. Synthesis, surface chemistry, and fluorescent properties of InP quantum dots. *Chem. Mater.* **35**, 822–836 (2023).
27. Kim, Y. et al. III–V colloidal nanocrystals: control of covalent surfaces. *Chem. Sci.* **11**, 913–922 (2020).

28. Jang, E., Kim, Y., Won, Y.-H., Jang, H. & Choi, S.-M. Environmentally friendly InP-based quantum dots for efficient wide color gamut displays. *ACS Energy Lett.* **5**, 1316–1327 (2020).
29. Wu, Z., Liu, P., Zhang, W., Wang, K. & Sun, X. W. Development of InP quantum dot-based light-emitting diodes. *ACS Energy Lett.* **5**, 1095–1106 (2020).
30. Adachi, S. *Handbook on Physical Properties of Semiconductors* Vol. 2 (Springer, 2004).
31. Abdollahi, A., Golzan, M. M. & Aghayar, K. First-principles investigation of electronic properties of AlxIn1−xP semiconductor alloy. *J. Mater. Sci.* **51**, 7343–7354 (2016).
32. Braunstein, R. & Kane, E. O. The valence band structure of the III–V compounds. *J. Phys. Chem. Solids* **23**, 1423–1431 (1962).
33. Vurgaftman, I., Meyer, J. R. & Ram-Mohan, L. R. Band parameters for III–V compound semiconductors and their alloys. *J. Appl. Phys.* **89**, 5815–5875 (2001).
34. Kim, Y.-S., Marsman, M., Kresse, G., Tran, F. & Blaha, P. Towards efficient band structure and effective mass calculations for III–V direct band-gap semiconductors. *Phys. Rev. B* **82**, 205212 (2010).
35. Almeida, G. et al. Size-dependent optical properties of InP CQDs. *Nano Lett.* https://doi.org/10.1021/acs.nanolett.3c02630 (2023).
36. Franceschetti, A., Fu, H., Wang, L. W. & Zunger, A. Many-body pseudopotential theory of excitons in InP and CdSe quantum dots. *Phys. Rev. B* **60**, 1819–1829 (1999).
37. Efros, A. L. & Rosen, M. The electronic structure of semiconductor nanocrystals. *Annu. Rev. Mater. Sci.* **30**, 475–521 (2000).
38. Dümbgen, K. C., Zito, J., Infante, I. & Hens, Z. Shape, electronic structure, and trap states in indium phosphide quantum dots. *Chem. Mater.* **33**, 6885–6896 (2021).
39. Krauss, T. D. & Wise, F. W. Coherent acoustic phonons in a semiconductor quantum dot. *Phys. Rev. Lett.* **79**, 5102–5105 (1997).
40. Besombes, L., Kheng, K., Marsal, L. & Mariette, H. Acoustic phonon broadening mechanism in single quantum dot emission. *Phys. Rev. B* **63**, 155307 (2001).
41. Masumoto, Y. & Takagahara, T. (eds) *Semiconductor Quantum Dots: Physics, Spectroscopy and Applications* (Springer, 2002).
42. Bozyigit, D. et al. Soft surfaces of nanomaterials enable strong phonon interactions. *Nature* **531**, 618–622 (2016).
43. Cui, J. et al. Evolution of the single-nanocrystal photoluminescence linewidth with size and shell: implications for exciton–phonon coupling and the optimization of spectral linewidths. *Nano Lett.* **16**, 289–296 (2016).
44. Kirschner, M. S. et al. Transient melting and recrystallization of semiconductor nanocrystals under multiple electron–hole pair excitation. *Nano Lett.* **17**, 5314–5320 (2017).
45. Yazdani, N. et al. Tuning electron–phonon interactions in nanocrystals through surface termination. *Nano Lett.* **18**, 2233–2242 (2018).
46. Yazdani, N., Volk, S., Yarema, O., Yarema, M. & Wood, V. Size, ligand, and defect-dependent electron–phonon coupling in chalcogenide and perovskite nanocrystals and its impact on luminescence line widths. *ACS Photon.* **7**, 1088–1095 (2020).
47. Kang, S., Kim, Y., Jang, E., Kang, Y. & Han, S. Fundamental limit of emission linewidth of quantum dots: ab initio study on CdSe nanocrystals. *ACS Appl. Mater. Interfaces* **12**, 22012–22018 (2020).
48. Guzelturk, B. et al. Dynamic lattice distortions driven by surface trapping in semiconductor nanocrystals. *Nat. Commun.* **12**, 1860 (2021).
49. Monreal, R. C. Electron–phonon interaction in the dynamics of trap filling in quantum dots. *Phys. Rev. B* **104**, 184304 (2021).
50. Kim, J., Wong, C. Y. & Scholes, G. D. Exciton fine structure and spin relaxation in semiconductor colloidal quantum dots. *Acc. Chem. Res.* **42**, 1037–1046 (2009).
51. Brodu, A. et al. Exciton fine structure and lattice dynamics in InP/ZnSe core/shell quantum dots. *ACS Photon.* **5**, 3353–3362 (2018).
52. Brodu, A. et al. Fine structure of nearly isotropic bright excitons in InP/ZnSe colloidal quantum dots. *J. Phys. Chem. Lett.* **10**, 5468–5475 (2019).
53. Brodu, A. et al. Hyperfine interactions and slow spin dynamics in quasi-isotropic InP-based core/shell colloidal nanocrystals. *ACS Nano* **13**, 10201–10209 (2019).
54. Efros, A. L. et al. Band-edge exciton in quantum dots of semiconductors with a degenerate valence band: dark and bright exciton states. *Phys. Rev. B* **54**, 4843–4856 (1996).
55. Melnychuk, C. & Guyot-Sionnest, P. Multicarrier dynamics in quantum dots. *Chem. Rev.* **4**, 2325–2372 (2021).
56. Takagahara, T. Electron–phonon interactions and excitonic dephasing in semiconductor nanocrystals. *Phys. Rev. Lett.* **71**, 3577–3580 (1993).
57. Borri, P. et al. Exciton dephasing via phonon interactions in InAs quantum dots: dependence on quantum confinement. *Phys. Rev. B* **71**, 115328 (2005).
58. Masia, F., Accanto, N., Langbein, W. & Borri, P. Spin-flip limited exciton dephasing in CdSe/ZnS colloidal quantum dots. *Phys. Rev. Lett.* **108**, 087401 (2012).
59. Accanto, N. et al. Engineering the spin–flip limited exciton dephasing in colloidal CdSe/CdS quantum dots. *ACS Nano* **6**, 5227–5233 (2012).
60. Fumani, A. K. & Berezovsky, J. Magnetic-field-dependent spin decoherence and dephasing in room-temperature CdSe nanocrystal quantum dots. *Phys. Rev. B* **88**, 155316 (2013).
61. Micic, O. I., Curtis, C. J., Jones, K. M., Sprague, J. R. & Nozik, A. J. Synthesis and characterization of InP quantum dots. *J. Phys. Chem.* **98**, 4966–4969 (1994).
62. Guzelian, A. A. et al. Synthesis of size-selected, surface-passivated InP nanocrystals. *J. Phys. Chem.* **100**, 7212–7219 (1996).
63. Mićić, O. I., Jones, K. M., Cahill, A. & Nozik, A. J. Optical, electronic, and structural properties of uncoupled and close-packed arrays of InP quantum dots. *J. Phys. Chem. B* **102**, 9791–9796 (1998).
64. Battaglia, D. & Peng, X. Formation of high quality InP and InAs nanocrystals in a noncoordinating solvent. *Nano Lett.* **2**, 1027–1030 (2002).
65. Talapin, D. V. et al. Synthesis and surface modification of amino-stabilized CdSe, CdTe and InP nanocrystals. *Colloids Surf. A Physicochem. Eng. Asp.* **202**, 145–154 (2002).
66. Gao, S., Lu, J., Chen, N., Zhao, Y. & Xie, Y. Aqueous synthesis of III–V semiconductor GaP and InP exhibiting pronounced quantum confinement. *Chem. Commun.* **24**, 3064–3065 (2002).
67. Jun, K.-W., Khanna, P. K., Hong, K.-B., Baeg, J.-O. & Suh, Y.-D. Synthesis of InP nanocrystals from indium chloride and sodium phosphide by solution route. *Mater. Chem. Phys.* **96**, 494–497 (2006).
68. Gerbec, J. A., Magana, D., Washington, A. & Strouse, G. F. Microwave-enhanced reaction rates for nanoparticle synthesis. *J. Am. Chem. Soc.* **127**, 15791–15800 (2005).
69. Xu, S., Kumar, S. & Nann, T. Rapid synthesis of high-quality InP nanocrystals. *J. Am. Chem. Soc.* **128**, 1054–1055 (2006).
70. Xie, R., Battaglia, D. & Peng, X. Colloidal InP nanocrystals as efficient emitters covering blue to near-infrared. *J. Am. Chem. Soc.* **129**, 15432–15433 (2007).
71. Li, L., Protière, M. & Reiss, P. Economic synthesis of high quality InP nanocrystals using calcium phosphide as the phosphorus precursor. *Chem. Mater.* **20**, 2621–2623 (2008).
72. Harris, D. K. & Bawendi, M. G. Improved precursor chemistry for the synthesis of III–V quantum dots. *J. Am. Chem. Soc.* **134**, 20211–20213 (2012).
73. Xu, Z. et al. Formation of size-tunable and nearly monodisperse InP nanocrystals: chemical reactions and controlled synthesis. *Chem. Mater.* **31**, 5331–5341 (2019).
74. Won, Y.-H. et al. Highly efficient and stable InP/ZnSe/ZnS quantum dot light-emitting diodes. *Nature* **575**, 634–638 (2019).
75. Achorn, O. B., Franke, D. & Bawendi, M. G. Seedless continuous injection synthesis of indium phosphide quantum dots as a route to large size and low size dispersity. *Chem. Mater.* **32**, 6532–6539 (2020).
76. Song, W.-S. et al. Amine-derived synthetic approach to color-tunable InP/ZnS quantum dots with high fluorescent qualities. *J. Nanopart. Res.* **15**, 1750 (2013).
77. Kim, K. et al. Halide–amine co-passivated indium phosphide colloidal quantum dots in tetrahedral shape. *Angew. Chem. Int. Ed.* **55**, 3714–3718 (2016).
78. Tessier, M. D., De Nolf, K., Dupont, D., Sinnaeve, D., De Roo, J. & Hens, Z. Aminophosphines: a double role in the synthesis of colloidal indium phosphide quantum dots. *J. Am. Chem. Soc.* **138**, 5923–5929 (2016).
79. Jo, J.-H. et al. InP-based quantum dots having an InP core, composition-gradient ZnSeS inner shell, and ZnS outer shell with sharp, bright emissivity, and blue absorptivity for display devices. *ACS Appl. Nano Mater.* **3**, 1972–1980 (2020).
80. Liu, Z. et al. Coreduction colloidal synthesis of III–V nanocrystals: the case of InP. *Angew. Chem. Int. Ed.* **47**, 3540–3542 (2008).
81. Joung, S., Yoon, S., Han, C.-S., Kim, Y. & Jeong, S. Facile synthesis of uniform large-sized InP nanocrystal quantum dots using tris(tert-butyldimethylsilyl)phosphine. *Nanoscale Res. Lett.* **7**, 93 (2012).
82. Gary, D. C., Glassy, B. A. & Cossairt, B. M. Investigation of indium phosphide quantum dot nucleation and growth utilizing triarylsilylphosphine precursors. *Chem. Mater.* **26**, 1734–1744 (2014).
83. Chandrasiri, H. B., Kim, E. B. & Snee, P. T. Sterically encumbered tris(trialkylsilyl) phosphine precursors for quantum dot synthesis. *Inorg. Chem.* **59**, 15928–15935 (2020).
84. Wells, R. L. et al. The use of tris(trimethylsilyl)arsine to prepare gallium arsenide and indium arsenide. *Chem. Mater.* **1**, 4–6 (1989).
85. Virieux, H. et al. InP/ZnS nanocrystals: coupling NMR and XPS for fine surface and interface description. *J. Am. Chem. Soc.* **134**, 19701–19708 (2012).
86. Ubbink, R. F. et al. In situ HF treatment for ultrabright InP quantum dots. *Chem. Mater.* **34**, 10093–10103 (2022).
87. Gary, D. C. & Cossairt, B. M. Role of acid in precursor conversion during InP quantum dot synthesis. *Chem. Mater.* **25**, 2463–2469 (2013).
88. Angelé, L., Dreyfuss, S., Dubertret, B. & Mézailles, N. Synthesis of monodisperse InP quantum dots: use of an acid-free indium carboxylate precursor. *Inorg. Chem.* **60**, 2271–2278 (2021).
89. Narayanaswamy, A., Xu, H., Pradhan, N., Kim, M. & Peng, X. Formation of nearly monodisperse In_2O_3 nanodots and oriented-attached nanoflowers: hydrolysis and alcoholysis vs pyrolysis. *J. Am. Chem. Soc.* **128**, 10310–10319 (2006).
90. Li, Y., Hou, X., Shen, Y., Dai, N. & Peng, X. Tuning the reactivity of indium alkanoates by tertiary organophosphines for the synthesis of indium-based quantum dots. *Chem. Mater.* **33**, 9348–9356 (2021).
91. Zhao, T. et al. General synthetic route to high-quality colloidal III–V semiconductor quantum dots based on pnictogen chlorides. *J. Am. Chem. Soc.* **141**, 15145–15152 (2019).
92. Ginterseder, M. et al. Scalable synthesis of InAs quantum dots mediated through indium redox chemistry. *J. Am. Chem. Soc.* **142**, 4088–4092 (2020).
93. Yadav, R. et al. Narrow near-infrared emission from InP QDs synthesized with indium(I) halides and aminophosphine. *J. Am. Chem. Soc.* **145**, 5070–5891 (2023).
94. Valleix, R. et al. Size-controlled indium phosphide quantum dots for bright and tunable light emission by simple hindered diamine addition. *ACS Appl. Nano Mater.* **4**, 11105–11114 (2021).
95. Xie, L., Harris, D. K., Bawendi, M. G. & Jensen, K. F. Effect of trace water on the growth of indium phosphide quantum dots. *Chem. Mater.* **27**, 5058–5063 (2015).
96. Baquero, E. A. et al. Synthesis of oxide-free InP quantum dots: surface control and H_2-assisted growth. *Chem. Mater.* **29**, 9623–9627 (2017).
97. Calvin, J. J., Kaufman, T. M., Sedlak, A. B., Crook, M. F. & Alivisatos, A. P. Observation of ordered organic capping ligands on semiconducting quantum dots via powder X-ray diffraction. *Nat. Commun.* **12**, 2663 (2021).
98. Allen, P. M., Walker, B. J. & Bawendi, M. G. Mechanistic insights into the formation of InP quantum dots. *Angew. Chem. Int. Ed.* **49**, 760–762 (2010).

99. Gary, D. C., Terban, M. W., Billinge, S. J. L. & Cossairt, B. M. Two-step nucleation and growth of InP quantum dots via magic-sized cluster intermediates. *Chem. Mater.* **27**, 1432–1441 (2015).
100. Cossairt, B. M. Shining light on indium phosphide quantum dots: understanding the interplay among precursor conversion, nucleation, and growth. *Chem. Mater.* **28**, 7181–7189 (2016).
101. Xie, L. et al. Characterization of indium phosphide quantum dot growth intermediates using MALDI-TOF mass spectrometry. *J. Am. Chem. Soc.* **138**, 13469–13472 (2016).
102. Gary, D. C., Petrone, A., Li, X. & Cossairt, B. M. Investigating the role of amine in InP nanocrystal synthesis: destabilizing cluster intermediates by Z-type ligand displacement. *Chem. Commun.* **53**, 161–164 (2017).
103. Friedfeld, M. R., Johnson, D. A. & Cossairt, B. M. Conversion of InP clusters to quantum dots. *Inorg. Chem.* **58**, 803–810 (2019).
104. Kwon, Y. et al. Evolution from unimolecular to colloidal-quantum-dot-like character in chlorine or zinc incorporated InP magic size clusters. *Nat. Commun.* **11**, 3127 (2020).
105. Gary, D. C. et al. Single-crystal and electronic structure of a 1.3 nm indium phosphide nanocluster. *J. Am. Chem. Soc.* **138**, 1510–1513 (2016).
106. McMurtry, B. M. et al. Continuous nucleation and size dependent growth kinetics of indium phosphide nanocrystals. *Chem. Mater*. https://doi.org/10.1021/acs.chemmater.0c01561 (2020).
107. Zhao, Q. & Kulik, H. J. Electronic structure origins of surface-dependent growth in III–V quantum dots. *Chem. Mater.* **30**, 7154–7165 (2018).
108. Baek, J., Allen, P. M., Bawendi, M. G. & Jensen, K. F. Investigation of indium phosphide nanocrystal synthesis using a high-temperature and high-pressure continuous flow microreactor. *Angew. Chem. Int. Ed.* **50**, 627–630 (2011).
109. Kim, K., Jeong, S., Woo, J. Y. & Han, C.-S. Successive and large-scale synthesis of InP/ZnS quantum dots in a hybrid reactor and their application to white LEDs. *Nanotechnology* **23**, 065602 (2012).
110. Ippen, C. et al. Large-scale synthesis of high quality InP quantum dots in a continuous flow-reactor under supercritical conditions. *Nanotechnology* **26**, 085604 (2015).
111. Baek, J., Shen, Y., Lignos, I., Bawendi, M. G. & Jensen, K. F. Multistage microfluidic platform for the continuous synthesis of III–V core/shell quantum dots. *Angew. Chem. Int. Ed.* **57**, 10915–10918 (2018).
112. Vikram, A. et al. Reactor system for multistep continuous synthesis of InP/ZnSeS nanoparticles. *ChemNanoMat* **4**, 943–953 (2018).
113. Lignos, I. et al. A high-temperature continuous stirred-tank reactor cascade for the multistep synthesis of InP/ZnS quantum dots. *React. Chem. Eng.* **6**, 459–464 (2021).
114. Okamoto, A. et al. Narrowing of the particle size distribution of InP quantum dots for green light emission by synthesis in micro-flow reactor. *ChemistrySelect* **7**, e202104215 (2022).
115. Kim, Y. et al. Tailored growth of single-crystalline InP tetrapods. *Nat. Commun.* **12**, 4454 (2021).
116. Yoo, H., Lee, K.-S., Nahm, S., Hwang, G. W. & Kim, S. Predicting ligand-dependent nanocrystal shapes of InP quantum dots and their electronic structures. *Appl. Surf. Sci.* **578**, 151972 (2022).
117. Micic, O. I. et al. Synthesis and characterization of InP, GaP, and $GaInP_2$ quantum dots. *J. Phys. Chem.* **99**, 7754–7759 (1995).
118. Kim, S.-W. et al. Engineering $InAs_xP_{1-x}$/InP/ZnSe III–V alloyed core/shell quantum dots for the near-infrared. *J. Am. Chem. Soc.* **127**, 10526–10532 (2005).
119. Joo, J. et al. Synthesis and characterization of $In_{1-x}Ga_xP$@ZnS alloy core–shell type colloidal quantum dots. *J. Ind. Eng. Chem.* **88**, 106–110 (2020).
120. Kim, Y., Yang, K. & Lee, S. Highly luminescent blue-emitting $In_{1-x}Ga_xP$@ZnS quantum dots and their applications in QLEDs with inverted structure. *J. Mater. Chem. C* **8**, 7679–7687 (2020).
121. Leemans, J. et al. Acid–base mediated ligand exchange on near-infrared absorbing, indium-based III–V colloidal quantum dots. *J. Am. Chem. Soc.* **143**, 4290–4301 (2021).
122. Yarema, M. & Kovalenko, M. V. Colloidal synthesis of InSb nanocrystals with controlled polymorphism using indium and antimony amides. *Chem. Mater.* **25**, 1788–1792 (2013).
123. De Trizio, L. et al. $Cu_{3-x}P$ nanocrystals as a material platform for near-infrared plasmonics and cation exchange reactions. *Chem. Mater.* **27**, 1120–1128 (2015).
124. Koh, S., Kim, W. D., Bae, W. K., Lee, Y. K. & Lee, D. C. Controlling ion-exchange balance and morphology in cation exchange from $Cu_{3-x}P$ nanoplatelets into InP crystals. *Chem. Mater.* **31**, 1990–2001 (2019).
125. Stone, D. et al. Luminescent anisotropic wurtzite InP nanocrystals. *Nano Lett.* **21**, 10032–10039 (2021).
126. Shan, X., Li, B. & Ji, B. Synthesis of wurtzite In and Ga phosphide quantum dots through cation exchange reactions. *Chem. Mater.* **33**, 5223–5232 (2021).
127. Choi, M.-J. et al. Ligand exchange at a covalent surface enables balanced stoichiometry in III–V colloidal quantum dots. *Nano Lett.* **21**, 6057–6063 (2021).
128. Zhao, T. et al. Engineering the surface chemistry of colloidal InP quantum dots for charge transport. *Chem. Mater.* **34**, 8306–8315 (2022).
129. Boles, M. A., Ling, D., Hyeon, T. & Talapin, D. V. The surface science of nanocrystals. *Nat. Mater.* **15**, 141–153 (2016).
130. Ghosh, S. & Manna, L. The many 'facets' of halide ions in the chemistry of colloidal inorganic nanocrystals. *Chem. Rev.* **118**, 7804–7864 (2018).
131. Wang, W. et al. Colloidal inorganic ligand-capped nanocrystals: fundamentals, status, and insights into advanced functional nanodevices. *Chem. Rev.* **122**, 4091–4162 (2022).
132. Rosenberg, A. J. The oxidation of intermetallic compounds — III: the room-temperature oxidation of AIIIBv compounds. *J. Phys. Chem. Solids* **14**, 175–180 (1960).
133. Hollinger, G., Bergignat, E., Joseph, J. & Robach, Y. On the nature of oxides on InP surfaces. *J. Vac. Sci. Technol. A* **3**, 2082–2088 (1985).
134. Mićić, O. I., Sprague, J., Lu, Z. & Nozik, A. J. Highly efficient band-edge emission from InP quantum dots. *Appl. Phys. Lett.* **68**, 3150–3152 (1996).
135. Cros-Gagneux, A. et al. Surface chemistry of InP quantum dots: a comprehensive study. *J. Am. Chem. Soc.* **132**, 18147–18157 (2010).
136. Cossairt, B. M., Stein, J. L., Holden, W. M. & Seidler, G. T. 4-1: Invited paper: role of phosphorus oxidation in controlling the luminescent properties of indium phosphide quantum dots. *SID Symposium Digest of Technical Papers* **49**, 21–24 (2018).
137. Clarke, M. T. et al. Synthesis of super bright indium phosphide colloidal quantum dots through thermal diffusion. *Commun. Chem.* **2**, 36 (2019).
138. Vikram, A. et al. Unraveling the origin of interfacial oxidation of InP-based quantum dots: implications for bioimaging and optoelectronics. *ACS Appl. Nano Mater.* **3**, 12325–12333 (2020).
139. Yang, W. et al. Surface passivation extends single and biexciton lifetimes of InP quantum dots. *Chem. Sci.* **11**, 5779–5789 (2020).
140. Pu, Y.-C., Fan, H.-C., Chang, J.-C., Chen, Y.-H. & Tseng, S.-W. Effects of interfacial oxidative layer removal on charge carrier recombination dynamics in InP/$ZnSe_xS_{1-x}$ core/shell quantum dots. *J. Phys. Chem. Lett.* **12**, 7194–7200 (2021).
141. Chen, G., Visbeck, S. B., Law, D. C. & Hicks, R. F. Structure-sensitive oxidation of the indium phosphide (001) surface. *J. Appl. Phys.* **91**, 9362–9367 (2002).
142. Santosh, K. et al. First principles study on InP (001)-(2×4) surface oxidation. *J. Appl. Phys.* **113**, 103705 (2013).
143. May, M. M., Lewerenz, H.-J. & Hannappel, T. Optical in situ study of InP(100) surface chemistry: dissociative adsorption of water and oxygen. *J. Phys. Chem. C* **118**, 19032–19041 (2014).
144. Ruiz Alvarado, I. A., Karmo, M., Runge, E. & Schmidt, W. G. InP and AlInP(001)(2 × 4) surface oxidation from density functional theory. *ACS Omega* **6**, 6297–6304 (2021).
145. Zhang, X., Ogitsu, T., Wood, B. C., Pham, T. A. & Ptasinska, S. Oxidation-induced polymerization of InP surface and implications for optoelectronic applications. *J. Phys. Chem. C* **123**, 30893–30902 (2019).
146. Wood, B. C., Schwegler, E., Choi, W. I. & Ogitsu, T. Surface chemistry of GaP(001) and InP(001) in contact with water. *J. Phys. Chem. C* **118**, 1062–1070 (2014).
147. Ramasamy, P., Kim, B., Lee, M.-S. & Lee, J.-S. Beneficial effects of water in the colloidal synthesis of InP/ZnS core–shell quantum dots for optoelectronic applications. *Nanoscale* **8**, 17159–17168 (2016).
148. Vikram, A. et al. Mechanistic insights into size-focused growth of indium phosphide nanocrystals in the presence of trace water. *Chem. Mater.* **32**, 3577–3584 (2020).
149. Baquero, E. A. et al. Identifying short surface ligands on metal phosphide quantum dots. *Phys. Chem. Chem. Phys.* **18**, 17330–17334 (2016).
150. Tomaselli, M. et al. NMR study of InP quantum dots: surface structure and size effects. *J. Chem. Phys.* **110**, 8861–8864 (1999).
151. Stein, J. L. et al. Probing surface defects of InP quantum dots using phosphorus Kα and Kβ X-ray emission spectroscopy. *Chem. Mater.* **30**, 6377–6388 (2018).
152. Calvin, J. J. et al. Thermodynamic investigation of increased luminescence in indium phosphide quantum dots by treatment with metal halide salts. *J. Am. Chem. Soc.* **142**, 18897–18906 (2020).
153. Protière, M. & Reiss, P. Amine-induced growth of an In_2O_3 shell on colloidal InP nanocrystals. *Chem. Commun.* **27**, 2417–2419 (2007).
154. Tessier, M. D. et al. Interfacial oxidation and photoluminescence of InP-Based core/shell quantum dots. *Chem. Mater.* **30**, 6877–6883 (2018).
155. Sadeghi, S. et al. Stokes-shift-engineered indium phosphide quantum dots for efficient luminescent solar concentrators. *ACS Appl. Mater. Interfaces* **10**, 12975–12982 (2018).
156. Kim, K. et al. Zinc oxo clusters improve the optoelectronic properties on indium phosphide quantum dots. *Chem. Mater.* **32**, 2795–2802 (2020).
157. Granada-Ramirez, D. A. et al. Chemical synthesis and optical, structural, and surface characterization of InP-In2O3 quantum dots. *Appl. Surf. Sci.* **530**, 147294 (2020).
158. Eren, G. O. et al. Cadmium-free and efficient type-II InP/ZnO/ZnS quantum dots and their application for LEDs. *ACS Appl. Mater. Interfaces* **13**, 32022–32030 (2021).
159. Van Avermaet, H. et al. Full-spectrum InP-based quantum dots with near-unity photoluminescence quantum efficiency. *ACS Nano* **6**, 9701–9712 (2022).
160. Wood, B. C., Ogitsu, T. & Schwegler, E. Local structural models of complex oxygen- and hydroxyl-rich GaP/InP (001) surfaces. *J. Chem. Phys.* **136**, 064705 (2012).
161. Wood, B. C., Schwegler, E., Choi, W. I. & Ogitsu, T. Surface chemistry of GaP (001) and InP (001) in contact with water. *J. Phys. Chem. C* **118**, 1062–1070 (2014).
162. Pham, T. A. et al. Integrating ab initio simulations and X-ray photoelectron spectroscopy: toward a realistic description of oxidized solid/liquid interfaces. *J. Phys. Chem. Lett.* **9**, 194–203 (2018).
163. Zhang, X., Pham, T. A., Ogitsu, T., Wood, B. C. & Ptasinska, S. Modulation of surface bonding topology: oxygen bridges on OH-terminated InP (001). *J. Phys. Chem. C* **124**, 3196–3203 (2020).
164. Ruiz Alvarado, I. A., Karmo, M., Runge, E. & Schmidt, W. G. InP and AlInP (001)(2× 4) surface oxidation from density functional theory. *ACS Omega* **6**, 6297–6304 (2021).
165. Berwanger, M., Schoenhalz, A. L., Dos Santos, C. L. & Piquini, P. Oxidation of InP nanowires: a first principles molecular dynamics study. *Phys. Chem. Chem. Phys.* **18**, 31101–31106 (2016).
166. Park, N. et al. Colloidal, room-temperature growth of metal oxide shells on InP quantum dots. *Inorg. Chem.* **62**, 6674–6687 (2023).

167. Gatos, H. C. & Lavine, M. C. Characteristics of the {111} surfaces of the III–V intermetallic compounds. *J. Electrochem. Soc.* **107**, 427 (1960).
168. Clark, D., Fok, T., Roberts, G. & Sykes, R. An investigation by electron spectroscopy for chemical analysis of chemical treatments of the (100) surface of n-type InP epitaxial layers for Langmuir film deposition. *Thin Solid Films* **70**, 261–283 (1980).
169. Adam, S. et al. The effect of nanocrystal surface structure on the luminescence properties: photoemission study of HF-etched InP nanocrystals. *J. Chem. Phys.* **123**, 084706 (2005).
170. Talapin, D. V. et al. Etching of colloidal InP nanocrystals with fluorides: photochemical nature of the process resulting in high photoluminescence efficiency. *J. Phys. Chem. B* **106**, 12659–12663 (2002).
171. Kim, T.-G. et al. Trap passivation in indium-based quantum dots through surface fluorination: mechanism and applications. *ACS Nano* **12**, 11529–11540 (2018).
172. Li, H. et al. ZnF_2-assisted synthesis of highly luminescent InP/ZnSe/ZnS quantum dots for efficient and stable electroluminescence. *Nano Lett.* **10**, 4067–4073 (2022).
173. Lovingood, D. D. & Strouse, G. F. Microwave induced in-situ active ion etching of growing InP nanocrystals. *Nano Lett.* **8**, 3394–3397 (2008).
174. Hughes, K. E., Stein, J. L., Friedfeld, M. R., Cossairt, B. M. & Gamelin, D. R. Effects of surface chemistry on the photophysics of colloidal InP nanocrystals. *ACS Nano* **13**, 14198–14207 (2019).
175. Fu, H. & Zunger, A. InP quantum dots: electronic structure, surface effects, and the redshifted emission. *Phys. Rev. B* **56**, 1496–1508 (1997).
176. Cho, E. et al. Optical characteristics of the surface defects in InP colloidal quantum dots for highly efficient light-emitting applications. *ACS Appl. Nano Mater.* **1**, 7106–7114 (2018).
177. Stein, J. L., Mader, E. A. & Cossairt, B. M. Luminescent InP quantum dots with tunable emission by post-synthetic modification with Lewis acids. *J. Phys. Chem. Lett.* **7**, 1315–1320 (2016).
178. Kirkwood, N. et al. Finding and fixing traps in II–VI and III–V colloidal quantum dots: the importance of Z-type ligand passivation. *J. Am. Chem. Soc.* **140**, 15712–15723 (2018).
179. Hanrahan, M. P., Stein, J. L., Park, N., Cossairt, B. M. & Rossini, A. J. Elucidating the location of Cd^{2+} in post-synthetically treated InP quantum dots using dynamic nuclear polarization 31P and 113Cd solid-state NMR spectroscopy. *J. Phys. Chem. C* **125**, 2956–2965 (2021).
180. Duke, C. Semiconductor surface reconstruction: the structural chemistry of two-dimensional surface compounds. *Chem. Rev.* **96**, 1237–1260 (1996).
181. Chadi, D. Vacancy-induced 2× 2 reconstruction of the Ga (111) surface of GaAs. *Phys. Rev. Lett.* **52**, 1911 (1984).
182. Chadi, D. Atomic structure of the (2× 2) reconstructed GaAs ($1^-\,1^-\,1^-$) surface: a multivacancy model. *Phys. Rev. Lett.* **57**, 102 (1986).
183. Biegelsen, D., Bringans, R., Northrup, J. & Swartz, L. Reconstructions of GaAs (1 1 1) surfaces observed by scanning tunneling microscopy. *Phys. Rev. Lett.* **65**, 452 (1990).
184. Voznyy, O. & Sargent, E. Atomistic model of fluorescence intermittency of colloidal quantum dots. *Phys. Rev. Lett.* **112**, 157401 (2014).
185. Schubert, E. F. *Doping in III–V Semiconductors* (Cambridge Univ. Press, 1993).
186. Thuy, U. T. D., Maurice, A., Liem, N. Q. & Reiss, P. Europium doped In(Zn)P/ZnS colloidal quantum dots. *Dalton Trans.* **42**, 12606–12610 (2013).
187. Xie, R. & Peng, X. Synthesis of Cu-doped InP nanocrystals (d-dots) with ZnSe diffusion barrier as efficient and color-tunable NIR emitters. *J. Am. Chem. Soc.* **131**, 10645–10651 (2009).
188. Knowles, K. E., Nelson, H. D., Kilburn, T. B. & Gamelin, D. R. Singlet–triplet splittings in the luminescent excited states of colloidal Cu+:CdSe, Cu+:InP, and $CuInS_2$ nanocrystals: charge-transfer configurations and self-trapped excitons. *J. Am. Chem. Soc.* **137**, 13138–13147 (2015).
189. Hassan, A., Zhang, X., Liu, C. & Snee, P. T. Electronic structure and dynamics of copper-doped indium phosphide nanocrystals studied with time-resolved X-ray absorption and large-scale DFT calculations. *J. Phys. Chem. C* **122**, 11145–11151 (2018).
190. Kim, H.-J. et al. Emission enhancement of Cu-doped InP quantum dots through double shelling scheme. *Materials* **12**, 2267 (2019).
191. Sadeghi, S. et al. High-performance, large-area, and ecofriendly luminescent solar concentrators using copper-doped InP quantum dots. *iScience* **23**, 101272 (2020).
192. Mundy, M. E., Eagle, F. W., Hughes, K. E., Gamelin, D. R. & Cossairt, B. M. Synthesis and spectroscopy of emissive, surface-modified, copper-doped indium phosphide nanocrystals. *ACS Mater. Lett.* **2**, 576–581 (2020).
193. Kim, J. et al. Highly luminescent near-infrared Cu-doped InP quantum dots with a Zn–Cu–In–S/ZnS double shell scheme. *J. Mater. Chem. C* **9**, 4330–4337 (2021).
194. Prins, P. T. et al. Slow hole localization and fast electron cooling in Cu-doped InP/ZnSe quantum dots. *J. Phys. Chem. Lett.* **13**, 9950–9956 (2022).
195. Thuy, U. T. D., Reiss, P. & Liem, N. Q. Luminescence properties of In(Zn)P alloy core/ZnS shell quantum dots. *Appl. Phys. Lett.* **97**, 193104 (2010).
196. Koh, S. et al. Zinc–phosphorus complex working as an atomic valve for colloidal growth of monodisperse indium phosphide quantum dots. *Chem. Mater.* **29**, 6346–6355 (2017).
197. Suh, Y.-H. et al. Engineering core size of InP quantum dot with incipient ZnS for blue emission. *Adv. Optical Mater.* **10**, 2102372 (2022).
198. Mahajan, S., Bonner, W. A., Chin, A. K. & Miller, D. C. The characterization of highly-zinc-doped InP crystals. *Appl. Phys. Lett.* **35**, 165–168 (1979).
199. van Gurp, G. J., van Dongen, T., Fontijn, G. M., Jacobs, J. M. & Tjaden, D. L. A. Interstitial and substitutional Zn in InP and InGaAsP. *J. Appl. Phys.* **65**, 553–560 (1989).
200. Janke, E. M. et al. Origin of broad emission spectra in InP quantum dots: contributions from structural and electronic disorder. *J. Am. Chem. Soc.* **140**, 15791–15803 (2018).
201. Asor, L. et al. InAs nanocrystals with robust p-type doping. *Adv. Funct. Mater.* **31**, 2007456 (2021).
202. Asor, L. et al. Zn-doped P-type InAs nanocrystal quantum dots. *Adv. Mater.* **35**, 2208332 (2022).
203. Kirkwood, N. et al. Locating and controlling the Zn content in In(Zn)P quantum dots. *Chem. Mater.* **32**, 557–565 (2020).
204. Shen, C. et al. Highly luminescent InP–In(Zn)P/ZnSe/ZnS core/shell/shell colloidal quantum dots with tunable emissions synthesized based on growth-doping. *J. Mater. Chem. C* **9**, 9599–9609 (2021).
205. Kim, Y. et al. Bright and uniform green light emitting InP/ZnSe/ZnS quantum dots for wide color gamut displays. *ACS Appl. Nano Mater.* **2**, 1496–1504 (2019).
206. Liu, P. et al. Green InP/ZnSeS/ZnS core multi-shelled quantum dots synthesized with aminophosphine for effective display applications. *Adv. Funct. Mater.* **31**, 2008453 (2021).
207. Zhang, W. et al. High quantum yield blue InP/ZnS/ZnS quantum dots based on bromine passivation for efficient blue light-emitting diodes. *Adv. Optical Mater.* **10**, 2200685 (2022).
208. Yu, P. et al. Highly efficient green InP-based quantum dot light-emitting diodes regulated by inner alloyed shell component. *Light Sci. Appl.* **11**, 162 (2022).
209. Heun, S. et al. Interface composition and stacking fault density in II–VI/III–V heterostructures. *Appl. Phys. Lett.* **70**, 237–239 (1997).
210. Colli, A., Pelucchi, E. & Franciosi, A. Controlling the native stacking fault density in II–VI/III–V heterostructures. *Appl. Phys. Lett.* **83**, 81–83 (2003).
211. Kley, A. & Neugebauer, J. Atomic and electronic structure of the GaAs/ZnSe(001) interface. *Phys. Rev. B* **50**, 8616–8628 (1994).
212. Stroppa, A. & Peressi, M. ZnSe/GaAs(001) heterostructures with defected interfaces: structural, thermodynamic, and electronic properties. *Phys. Rev. B* **72**, 245304 (2005).
213. Colli, A., Carlino, E., Pelucchi, E., Grillo, V. & Franciosi, A. Local interface composition and native stacking fault density in ZnSe/GaAs(001) heterostructures. *J. Appl. Phys.* **96**, 2592–2602 (2004).
214. Deng, H.-X., Luo, J.-W. & Wei, S.-H. Chemical trends of stability and band alignment of lattice-matched II–VI/III–V semiconductor interfaces. *Phys. Rev. B* **91**, 075315 (2015).
215. Park, N. et al. Tuning the interfacial stoichiometry of InP core and InP/ZnSe core/shell quantum dots. *J. Chem. Phys.* **155**, 084701 (2021).
216. Cho, D.-Y., Xi, L., Boothroyd, C., Kardynal, B. & Lam, Y. M. The role of ion exchange in the passivation of In(Zn)P nanocrystals with ZnS. *Sci. Rep.* **6**, 22818 (2016).
217. Li, Y. et al. Stoichiometry-controlled InP-based quantum dots: synthesis, photoluminescence, and electroluminescence. *J. Am. Chem. Soc.* **141**, 6448–6452 (2019).
218. Sun, Z. et al. Suppressing the cation exchange at the core/shell interface of InP quantum dots by a selenium shielding layer enables efficient green light-emitting diodes. *ACS Appl. Mater. Interfaces* **14**, 15401–15406 (2022).
219. Wu, Q. et al. Quasi-shell-growth strategy achieves stable and efficient green InP quantum dot light-emitting diodes. *Adv. Sci.* **9**, 2200959 (2022).
220. Park, N. & Cossairt, B. Colloidal, room temperature growth of metal oxide shells on InP quantum dots. *Inorg. Chem.* **62**, 6674–6687 (2023).
221. Jang, Y. et al. Interface control of electronic and optical properties in IV–VI and II–VI core/shell colloidal quantum dots: a review. *Chem. Commun.* **53**, 1002–1024 (2017).
222. Chen, X., Lou, Y., Samia, A. C. & Burda, C. Coherency strain effects on the optical response of core/shell heteronanostructures. *Nano Lett.* **3**, 799–803 (2003).
223. Jing, L. et al. Insight into strain effects on band alignment shifts, carrier localization and recombination kinetics in CdTe/CdS core/shell quantum dots. *J. Am. Chem. Soc.* **137**, 2073–2084 (2015).
224. Smith, A. M., Mohs, A. M. & Nie, S. Tuning the optical and electronic properties of colloidal nanocrystals by lattice strain. *Nat. Nanotechnol.* **4**, 56–63 (2009).
225. Han, P. & Bester, G. Heavy strain conditions in colloidal core–shell quantum dots and their consequences on the vibrational properties from ab initio calculations. *Phys. Rev. B* **92**, 125438 (2015).
226. Park, S.-H. & Cho, Y.-H. Strain and piezoelectric potential effects on optical properties in CdSe/CdS core/shell quantum dots. *J. Appl. Phys.* **109**, 113103 (2011).
227. Yablonovitch, E. & Kane, E. Reduction of lasing threshold current density by the lowering of valence band effective mass. *J. Lightwave Technol.* **4**, 504–506 (1986).
228. Fan, F. et al. Continuous-wave lasing in colloidal quantum dot solids enabled by facet-selective epitaxy. *Nature* **544**, 75–79 (2017).
229. Park, Y.-S., Lim, J. & Klimov, V. I. Asymmetrically strained quantum dots with non-fluctuating single-dot emission spectra and subthermal room-temperature linewidths. *Nat. Mater.* **18**, 249–255 (2019).
230. Wang, L. et al. Controlling the emission linewidths of alloy quantum dots with asymmetric strain. *J. Colloid Interface Sci.* **624**, 287–295 (2022).
231. Song, Y. et al. Enhanced emission directivity from asymmetrically strained colloidal quantum dots. *Sci. Adv.* **8**, eabl8219 (2022).
232. Kobayashi, T., Aoki, K. & Yamamoto, K. Pressure dependence of optical absorption in InP at 77 K. *Phys. B+C* **139–140**, 537–540 (1986).
233. Gorczyca, I., Christensen, N. E. & Alouani, M. Calculated optical and structural properties of InP under pressure. *Phys. Rev. B* **39**, 7705–7712 (1989).
234. Lee, C.-J., Mizel, A., Banin, U., Cohen, M. L. & Alivisatos, A. P. Observation of pressure-induced direct-to-indirect band gap transition in InP nanocrystals. *J. Chem. Phys.* **113**, 2016–2020 (2000).
235. Díaz, J. G., Bryant, G. W., Jaskólski, W. & Zieliński, M. Theory of InP nanocrystals under pressure. *Phys. Rev. B* **75**, 245433 (2007).
236. Liu, H. et al. Pressure-stimulus-responsive behaviors of core–shell InP/ZnSe nanocrystals: remarkable piezochromic luminescence and structural assembly. *Nanoscale* **14**, 7530–7537 (2022).

237. Rafipoor, M. et al. Strain engineering in InP/(Zn,Cd)Se core/shell quantum dots. *Chem. Mater.* **30**, 4393–4400 (2018).
238. Rafipoor, M. et al. Strain in InP/ZnSe, S core/shell quantum dots from lattice mismatch and shell thickness — material stiffness influence. *J. Chem. Phys.* **151**, 154704 (2019).
239. Frederick, M. T., Amin, V. A., Cass, L. C. & Weiss, E. A. A molecule to detect and perturb the confinement of charge carriers in quantum dots. *Nano Lett.* **11**, 5455–5460 (2011).
240. Harrison, W. A. & Tersoff, J. Tight-binding theory of heterojunction band lineups and interface dipoles. *J. Vac. Sci. Technol. B* **4**, 1068–1073 (1986).
241. Jeong, B. G. et al. Interface polarization in heterovalent core–shell nanocrystals. *Nat. Mater.* **21**, 246–252 (2021).
242. Hahm, D. et al. Design principle for bright, robust, and color-pure InP/$ZnSe_xS_{1-x}$/ZnS heterostructures. *Chem. Mater.* **31**, 3476–3484 (2019).
243. Zhang, W. et al. InP/ZnS/ZnS core/shell blue quantum dots for efficient light-emitting diodes. *Adv. Funct. Mater.* **30**, 2005303 (2020).
244. Mulder, J. T. et al. Developing lattice matched ZnMgSe shells on InZnP quantum dots for phosphor applications. *ACS Appl. Nano Mater.* **3**, 3859–3867 (2020).
245. Orfield, N. J., McBride, J. R., Keene, J. D., Davis, L. M. & Rosenthal, S. J. Correlation of atomic structure and photoluminescence of the same quantum dot: pinpointing surface and internal defects that inhibit photoluminescence. *ACS Nano* **9**, 831–839 (2015).
246. Kim, T. et al. Efficient and stable blue quantum dot light-emitting diode. *Nature* **586**, 385–389 (2020).
247. Cavanaugh, P. et al. Raman study of shell morphology in InP/ZnSe/ZnS core/shell/shell nanocrystals. *J. Phys. Chem. C* **125**, 10549–10557 (2021).
248. Nguyen, A. T., Jen-La Plante, I., Ippen, C., Ma, R. & Kelley, D. F. Extremely slow trap-mediated hole relaxation in room-temperature InP/ZnSe/ZnS quantum dots. *J. Phys. Chem. C* **125**, 4110–4118 (2021).
249. Cavanaugh, P. et al. Radiative dynamics and delayed emission in pure and doped InP/ZnSe/ZnS quantum dots. *J. Chem. Phys.* **155**, 244705 (2021).
250. Nguyen, A. T. et al. Auger dynamics in InP/ZnSe/ZnS quantum dots having pure and doped shells. *J. Phys. Chem. C* **125**, 15405–15414 (2021).
251. Sun, H. et al. Biexciton and trion dynamics in InP/ZnSe/ZnS quantum dots. *J. Chem. Phys.* **156**, 054703 (2022).
252. Kim, T., Won, Y.-H., Jang, E. & Kim, D. Negative trion auger recombination in highly luminescent InP/ZnSe/ZnS quantum dots. *Nano Lett.* **21**, 2111–2116 (2021).
253. Lee, S. H. et al. The effects of discrete and gradient mid-shell structures on the photoluminescence of single InP quantum dots. *Nanoscale* **11**, 23251–23258 (2019).
254. Lee, Y. et al. Effectual interface and defect engineering for auger recombination suppression in bright InP/ZnSeS/ZnS quantum dots. *ACS Appl. Mater. Interfaces* **14**, 12479–12487 (2022).
255. Sousa Velosa, F. et al. State filling and stimulated emission by colloidal InP/ZnSe core/shell quantum dots. *Adv. Optical Mater.* **10**, 2200328 (2022).
256. Kelley, A. M. et al. Identity of the reversible hole traps in InP/ZnSe core/shell quantum dots. *J. Chem. Phys.* **157**, 174701 (2022).
257. Cragg, G. E. & Efros, A. L. Suppression of auger processes in confined structures. *Nano Lett.* **10**, 313–317 (2010).
258. García-Santamaría, F. et al. Breakdown of volume scaling in auger recombination in CdSe/CdS heteronanocrystals: the role of the core–shell interface. *Nano Lett.* **11**, 687–693 (2011).
259. Park, Y.-S., Lim, J., Makarov, N. S. & Klimov, V. I. Effect of interfacial alloying versus 'volume scaling' on auger recombination in compositionally graded semiconductor quantum dots. *Nano Lett.* **17**, 5607–5613 (2017).
260. Lim, J., Park, Y.-S., Wu, K., Yun, H. J. & Klimov, V. I. Droop-free colloidal quantum dot light-emitting diodes. *Nano Lett.* **18**, 6645–6653 (2018).
261. Park, Y.-S., Bae, W. K., Baker, T., Lim, J. & Klimov, V. I. Effect of auger recombination on lasing in heterostructured quantum dots with engineered core/shell interfaces. *Nano Lett.* **15**, 7319–7328 (2015).
262. Roh, J., Park, Y.-S., Lim, J. & Klimov, V. I. Optically pumped colloidal-quantum-dot lasing in LED-like devices with an integrated optical cavity. *Nat. Commun.* **11**, 271 (2020).
263. Al-Ghamdi, M. S. et al. Absorption, gain, and threshold in InP/AlGaInP quantum dot laser diodes. *IEEE J. Quantum Electron.* **49**, 389–394 (2013).
264. Chen, C. H., Stockman, S. A., Peanasky, M. J. & Kuo, C. P. in *High Brightness Light Emitting Diodes* (eds Stringfellow, G. et al.) 97–149 (Elsevier, 1997).
265. Gessmann, T. & Schubert, E. F. High-efficiency AlGaInP light-emitting diodes for solid-state lighting applications. *J. Appl. Phys.* **95**, 2203–2216 (2004).
266. Meier, L., Braun, C., Hannappel, T. & Schmidt, W. G. Band alignment at $Ga_xIn_{1-x}P/Al_yIn_{1-y}P$ alloy interfaces from hybrid density functional theory calculations. *Phys. Stat. Sol.* **258**, 2000463 (2021).
267. Zhang, X. H., Chua, S. J. & Fan, W. J. Band offsets at GaInP/AlGaInP(001) heterostructures lattice matched to GaAs. *Appl. Phys. Lett.* **73**, 1098–1100 (1998).
268. Srivastava, V. et al. Colloidal chemistry in molten salts: synthesis of luminescent $In_{1-x}Ga_xP$ and $In_{1-x}Ga_xAs$ quantum dots. *J. Am. Chem. Soc.* **140**, 12144–12151 (2018).
269. Wegner, K. D., Pouget, S., Ling, W. L., Carrière, M. & Reiss, P. Gallium — a versatile element for tuning the photoluminescence properties of InP quantum dots. *Chem. Commun.* **55**, 1663–1666 (2019).
270. Kim, K.-H. et al. Cation-exchange-derived InGaP alloy quantum dots toward blue emissivity. *Chem. Mater.* **32**, 3537–3544 (2020).
271. Kim, S. et al. Highly luminescent InP/GaP/ZnS nanocrystals and their application to white light-emitting diodes. *J. Am. Chem. Soc.* **134**, 3804–3809 (2012).
272. Lee, W. L. C., Kim, B., Choi, Y. & Chae, H. Synthesis of blue-emissive InP/GaP/ZnS quantum dots via controlling the reaction kinetics of shell growth and length of capping ligands. *Nanomaterials* **10**, 2171 (2020).
273. Xu, Y. et al. Preparation of highly stable and photoluminescent cadmium-free InP/GaP/ZnS core/shell quantum dots and application to quantitative immunoassay. *Part. Part. Syst. Charact.* **37**, 1900441 (2020).
274. Luo, W., Lin, L., Huang, J., Lin, Q. & Lau, K. M. Electrically pumped InP/GaAsP quantum dot lasers grown on (001) Si emitting at 750 nm. *Opt. Expr.* **30**, 40750–40755 (2022).
275. Xie, R., Chen, K., Chen, X. & Peng, X. InAs/InP/ZnSe core/shell/shell quantum dots as near-infrared emitters: bright, narrow-band, non-cadmium containing, and biocompatible. *Nano Res.* **1**, 457–464 (2008).
276. Enright, M. J. et al. Role of atomic structure on exciton dynamics and photoluminescence in NIR emissive InAs/InP/ZnSe quantum dots. *J. Phys. Chem. C* **126**, 7576–7587 (2022).
277. Wijaya, H. et al. Efficient near-infrared light-emitting diodes based on In(Zn)As–In(Zn)P–GaP–ZnS quantum dots. *Adv. Funct. Mater.* **30**, 1906483 (2020).
278. Zhao, X., Lim, L. J., Ang, S. S. & Tan, Z.-K. Efficient short-wave infrared light-emitting diodes based on heavy-metal-free quantum dots. *Adv. Mater.* **34**, 2206409 (2022).
279. Eychmüller, A., Mews, A. & Weller, H. A quantum dot quantum well: CdS/HgS/CdS. *Chem. Phys. Lett.* **208**, 59–62 (1993).
280. Jeong, B. G. et al. Colloidal spherical quantum wells with near-unity photoluminescence quantum yield and suppressed blinking. *ACS Nano* **10**, 9297–9305 (2016).
281. Nagamine, G. et al. Efficient optical gain in spherical quantum wells enabled by engineering biexciton interactions. *ACS Photon.* **7**, 2252–2264 (2020).
282. Rreza, I. et al. Performance of spherical quantum well down converters in solid state lighting. *ACS Appl. Mater. Interfaces* **13**, 12191–12197 (2021).
283. Cassidy, J. et al. Quantum shells boost the optical gain of lasing media. *ACS Nano* **16**, 3017–3026 (2022).
284. Saeboe, A. M. et al. Extending the near-infrared emission range of indium phosphide quantum dots for multiplexed in vivo imaging. *Nano Lett.* **21**, 3271–3279 (2021).
285. Kim, S. et al. Reverse type-I ZnSe/InP/ZnS core/shell/shell nanocrystals: cadmium-free quantum dots for visible luminescence. *Small* **7**, 70–73 (2011).
286. Kim, S. et al. Bandgap engineered reverse type-I CdTe/InP/ZnS core–shell nanocrystals for the near-infrared. *Chem. Commun.* **10**, 1267–1269 (2009).
287. Kim, S. et al. Near-infrared fluorescent type II quantum dots for sentinel lymph node mapping. *Nat. Biotechnol.* **22**, 93–97 (2004).
288. Kim, S., Fisher, B., Eisler, H.-J. & Bawendi, M. Type-II quantum dots: CdTe/CdSe (core/shell) and CdSe/ZnTe (core/shell) heterostructures. *J. Am. Chem. Soc.* **125**, 11466–11467 (2003).
289. de Mello Donegá, C. Formation of nanoscale spatially indirect excitons: evolution of the type-II optical character of CdTe/CdSe heteronanocrystals. *Phys. Rev. B* **81**, 165303 (2010).
290. Gur, I., Fromer, N. A., Geier, M. L. & Alivisatos, A. P. Air-stable all-inorganic nanocrystal solar cells processed from solution. *Science* **310**, 462–465 (2005).
291. Simi, N. J., Bernadsha, S. B., Thomas, A. & Ison, V. V. Quantum dot sensitized solar cells using type-II CdSe-Cu2Se core–shell QDs. *Results Opt.* **4**, 100088 (2021).
292. Li, X. et al. Rational design of colloidal AgGaS2/CdSeS core/shell quantum dots for solar energy conversion and light detection. *Nano Energy* **89**, 106392 (2021).
293. Wang, Y. et al. Visible light driven type II heterostructures and their enhanced photocatalysis properties: a review. *Nanoscale* **5**, 8326–8339 (2013).
294. Zhou, Y., Zhao, H., Ma, D. & Rosei, F. Harnessing the properties of colloidal quantum dots in luminescent solar concentrators. *Chem. Soc. Rev.* **47**, 5866–5890 (2018).
295. Klimov, V. I. et al. Single-exciton optical gain in semiconductor nanocrystals. *Nature* **447**, 441–446 (2007).
296. Liao, C. et al. Ultralow-threshold single-mode lasing from phase-pure CdSe/CdS core/shell quantum dots. *J. Phys. Chem. Lett.* **7**, 4968–4976 (2016).
297. Dennis, A. M. et al. Suppressed blinking and auger recombination in near-infrared type-II InP/CdS nanocrystal quantum dots. *Nano Lett.* **12**, 5545–5551 (2012).
298. Wu, K. et al. Interfacial charge separation and recombination in InP and quasi-type II InP/CdS core/shell quantum dot-molecular acceptor complexes. *J. Phys. Chem. A* **117**, 7561–7570 (2013).
299. Smith, C. T. et al. Multiple exciton generation and dynamics in InP/CdS colloidal quantum dots. *J. Phys. Chem. C* **121**, 2099–2107 (2017).
300. Son, M., Kim, S., Lee, Y. & Bang, J. Synthesis of near-infrared-emitting type-II In(Zn)P/ZnTe (core/shell) quantum dots. *J. Alloy Compd.* **886**, 161233 (2021).
301. Karatum, O. et al. Light-emitting devices based on type-II InP/ZnO quantum dots. *ACS Photon.* **6**, 939–946 (2019).
302. Bahmani Jalali, H. et al. Effective neural photostimulation using indium-based type-II quantum dots. *ACS Nano* **12**, 8104–8114 (2018).
303. Karatum, O. et al. Quantum dot and electron acceptor nano-heterojunction for photo-induced capacitive charge-transfer. *Sci. Rep.* **11**, 2460 (2021).
304. Shimizu, K. T. et al. Toward commercial realization of quantum dot based white light-emitting diodes for general illumination. *Photon. Res.* **5**, A1–A6 (2017).
305. Toufanian, R., Chern, M., Kong, V. H. & Dennis, A. M. Engineering brightness-matched indium phosphide quantum dots. *Chem. Mater.* **33**, 1964–1975 (2021).
306. Dupont, D., Tessier, M. D., Smet, P. F. & Hens, Z. Indium phosphide-based quantum dots with shell-enhanced absorption for luminescent down-conversion. *Adv. Mater.* **29**, 1700686 (2017).
307. Karadza, B., Van Avermaet, H., Mingabudinova, L., Hens, Z. & Meuret, Y. Efficient, high-CRI white LEDs by combining traditional phosphors with cadmium-free InP/ZnSe red quantum dots. *Photon. Res.* **10**, 155–165 (2022).
308. Lee, S.-H. et al. Remote-type, high-color gamut white light-emitting diode based on InP quantum dot color converters. *Opt. Mater. Express* **4**, 1297–1302 (2014).
309. Tian, W., Dou, L., Jin, Z., Xiao, J. & Li, J. Full-color micro-LED displays with cadmium-free quantum dots patterned by photolithography technology. *Appl. Opt.* **59**, 11112–11122 (2020).

310. Boivin, D. B., Duffy, J. F., Kronauer, R. E. & Czeisler, C. A. Dose–response relationships for resetting of human circadian clock by light. *Nature* **379**, 540–542 (1996).
311. Pauley, S. M. Lighting for the human circadian clock: recent research indicates that lighting has become a public health issue. *Med. Hypotheses* **63**, 588–596 (2004).
312. Dong, K., Goyarts, E. C., Pelle, E., Trivero, J. & Pernodet, N. Blue light disrupts the circadian rhythm and create damage in skin cells. *Int. J. Cosmet. Sci.* **41**, 558–562 (2019).
313. Hye Oh, J., Ji Yang, S. & Rag Do, Y. Healthy, natural, efficient and tunable lighting: four-package white LEDs for optimizing the circadian effect, color quality and vision performance. *Light Sci. Appl.* **3**, e141 (2014).
314. Zhu, P., Zhu, H., Adhikari, G. C. & Thapa, S. Design of circadian white light-emitting diodes with tunable color temperature and nearly perfect color rendition. *OSA Contin.* **2**, 2413–2427 (2019).
315. Yang, J. et al. Toward full-color electroluminescent quantum dot displays. *Nano Lett.* **21**, 26–33 (2020).
316. Han, C.-Y. & Yang, H. Development of colloidal quantum dots for electrically driven light-emitting devices. *J. Korean Ceram. Soc.* **54**, 449–469 (2017).
317. Lim, J. et al. InP@ ZnSeS, core@ composition gradient shell quantum dots with enhanced stability. *Chem. Mater.* **23**, 4459–4463 (2011).
318. Lim, J. et al. Highly efficient cadmium-free quantum dot light-emitting diodes enabled by the direct formation of excitons within InP@ ZnSeS quantum dots. *ACS Nano* **7**, 9019–9026 (2013).
319. Jo, J.-H. et al. High-efficiency red electroluminescent device based on multishelled InP quantum dots. *Opt. Lett.* **41**, 3984–3987 (2016).
320. Cao, F. et al. Growth strategy for large-size InP/ZnSe/ZnS core–shell quantum dots enabling high-efficiency light-emitting diodes. *Chem. Mater.* **30**, 8002–8007 (2018).
321. Zhang, H. et al. High-efficiency green InP quantum dot-based electroluminescent device comprising thick-shell quantum dots. *Adv. Opt. Mater.* **7**, 1801602 (2019).
322. Iwasaki, Y., Motomura, G., Ogura, K. & Tsuzuki, T. Efficient green InP quantum dot light-emitting diodes using suitable organic electron-transporting materials. *Appl. Phys. Lett.* **117**, 111104 (2020).
323. Chao, W.-C. et al. High efficiency green InP quantum dot light-emitting diodes by balancing electron and hole mobility. *Commun. Mater.* **2**, 1–10 (2021).
324. Zhang, H. et al. High-brightness blue InP quantum dot-based electroluminescent devices: the role of shell thickness. *J. Phys. Chem. Lett.* **11**, 960–967 (2020).
325. Mei, G. et al. Light extraction employing optical tunneling in blue InP quantum dot light-emitting diodes. *Appl. Phys. Lett.* **120**, 091101 (2022).
326. Thimsen, E., Sadtler, B. & Berezin, M. Y. Shortwave-infrared (SWIR) emitters for biological imaging: a review of challenges and opportunities. *Nanophotonics* **6**, 1043–1054 (2017).
327. Yun, S. H. & Kwok, S. J. J. Light in diagnosis, therapy and surgery. *Nat. Biomed. Eng.* **1**, 0008 (2017).
328. Yao, J., Li, P., Li, L. & Yang, M. Biochemistry and biomedicine of quantum dots: from biodetection to bioimaging, drug discovery, diagnostics, and therapy. *Acta Biomater.* **74**, 36–55 (2018).
329. Zhao, P. et al. Near infrared quantum dots in biomedical applications: current status and future perspective. *Wiley Interdiscip. Rev. Nanomed. Nanobiotechnol.* **10**, e1483 (2018).
330. Lee, G.-H. et al. Multifunctional materials for implantable and wearable photonic healthcare devices. *Nat. Rev. Mater.* **5**, 149–165 (2020).
331. Teutsch, M., Sappa, A. D. & Hammoud, R. I. Computer vision in the infrared spectrum: challenges and approaches. *Synth. Lectures Comp. Vis.* **10**, 1–138 (2021).
332. Kahn, J. M. & Barry, J. R. Wireless infrared communications. *Proc. IEEE* **85**, 265–298 (1997).
333. Haffouz, S. et al. Bright single InAsP quantum dots at telecom wavelengths in position-controlled InP nanowires: the role of the photonic waveguide. *Nano Lett.* **18**, 3047–3052 (2018).
334. Lu, C.-Y. & Pan, J.-W. Quantum-dot single-photon sources for the quantum internet. *Nat. Nanotechnol.* **16**, 1294–1296 (2021).
335. Sargent, H. E. Infrared quantum dots. *Adv. Mater.* **17**, 515–522 (2005).
336. Lu, H., Carroll, G. M., Neale, N. R. & Beard, M. C. Infrared quantum dots: progress, challenges, and opportunities. *ACS Nano* **13**, 939–953 (2019).
337. Jin, D. et al. Nanoparticles for super-resolution microscopy and single-molecule tracking. *Nat. Methods* **15**, 415–423 (2018).
338. Chinnathambi, S. & Shirahata, N. Recent advances on fluorescent biomarkers of near-infrared quantum dots for in vitro and in vivo imaging. *Sci. Technol. Adv. Mater.* **20**, 337–355 (2019).
339. Tong, X., Wu, J. & Wang, Z. M. *Quantum Dot Photodetectors* (Springer, 2021).
340. Carey, G. H. et al. Colloidal quantum dot solar cells. *Chem. Rev.* **115**, 12732–12763 (2015).
341. Zhang, L. et al. In vivo tumor active cancer targeting and CT-fluorescence dual-modal imaging with nanoprobe based on gold nanorods and InP/ZnS quantum dots. *J. Mater. Chem. B* **6**, 2574–2583 (2018).
342. Zaban, A., Mićić, O. I., Gregg, B. A. & Nozik, A. J. Photosensitization of nanoporous TiO_2 electrodes with InP quantum dots. *Langmuir* **14**, 3153–3156 (1998).
343. Yang, S., Zhao, P., Zhao, X., Qu, L. & Lai, X. InP and Sn:InP based quantum dot sensitized solar cells. *J. Mater. Chem. A* **3**, 21922–21929 (2015).
344. Leemans, J. et al. Colloidal III–V quantum dot photodiodes for short-wave infrared photodetection. *Adv. Sci.* **9**, 2200844 (2022).
345. Lai, R., Sang, Y., Zhao, Y. & Wu, K. Triplet sensitization and photon upconversion using InP-based quantum dots. *J. Am. Chem. Soc.* **142**, 19825–19829 (2020).
346. Klimov, V. I. et al. Optical gain and stimulated emission in nanocrystal quantum dots. *Science* **290**, 314–317 (2000).
347. Geuchies, J. J. et al. Quantitative electrochemical control over optical gain in quantum-dot solids. *ACS Nano* **15**, 377–386 (2020).
348. Gao, S. et al. Lasing from colloidal InP/ZnS quantum dots. *Opt. Expr.* **19**, 5528–5535 (2011).
349. Senellart, P., Solomon, G. & White, A. High-performance semiconductor quantum-dot single-photon sources. *Nat. Nanotechnol.* **12**, 1026–1039 (2017).
350. Michler, P. *Quantum Dots for Quantum Information Technologies* (Springer Cham, 2017).
351. Benson, O., Santori, C., Pelton, M. & Yamamoto, Y. Regulated and entangled photons from a single quantum dot. *Phys. Rev. Lett.* **84**, 2513–2516 (2000).
352. Schimpf, C. et al. Quantum dots as potential sources of strongly entangled photons: perspectives and challenges for applications in quantum networks. *Appl. Phys. Lett.* **118**, 100502 (2021).
353. Trivedi, R., Fischer, K. A., Vučković, J. & Müller, K. Generation of non-classical light using semiconductor quantum dots. *Adv. Quantum Technol.* **3**, 1900007 (2020).
354. Akopian, N. et al. Entangled photon pairs from semiconductor quantum dots. *Phys. Rev. Lett.* **96**, 130501 (2006).
355. Lettner, T. et al. Strain-controlled quantum dot fine structure for entangled photon generation at 1550 nm. *Nano Lett.* **21**, 10501–10506 (2021).
356. Banin, U. et al. Quantum confinement and ultrafast dephasing dynamics in InP nanocrystals. *Phys. Rev. B* **55**, 7059–7067 (1997).
357. Ellingson, R. J. et al. Theoretical and experimental investigation of electronic structure and relaxation of colloidal nanocrystalline indium phosphide quantum dots. *Phys. Rev. B* **67**, 075308 (2003).
358. Narayanaswamy, A., Feiner, L. F., Meijerink, A. & van der Zaag, P. J. The effect of temperature and dot size on the spectral properties of colloidal InP/ZnS core–shell quantum dots. *ACS Nano* **3**, 2539–2546 (2009).
359. Huang, T. et al. Phonon induced pure dephasing process of excitonic state in colloidal semiconductor quantum dots. *Superlatt. Microstruct.* **92**, 52–59 (2016).
360. Brodu, A. et al. Exciton–phonon coupling in InP quantum dots with ZnS and (Zn, Cd) shells. *Phys. Rev. B* **101**, 125413 (2020).
361. Chandrasekaran, V. et al. Nearly blinking-free, high-purity single-photon emission by colloidal InP/ZnSe quantum dots. *Nano Lett.* **17**, 6104–6109 (2017).
362. Rainò, G. et al. Superfluorescence from lead halide perovskite quantum dot superlattices. *Nature* **563**, 671–675 (2018).
363. Grim, J. Q. et al. Scalable in operando strain tuning in nanophotonic waveguides enabling three-quantum-dot superradiance. *Nat. Mater.* **18**, 963–969 (2019).
364. Kim, T. et al. Shape-tuned multi-photon emitting InP nanotetrapod. *Adv. Mater.* **34**, 2110665 (2022).
365. Kwok, N. *Complete Guide to Semiconductor Devices* (Wiley–IEEE Press, 2002).
366. Van de Walle, C. G. & Neugebauer, J. Universal alignment of hydrogen levels in semiconductors, insulators and solutions. *Nature* **423**, 626–628 (2003).
367. Adachi, S. *The Handbook on Optical Constants of Semiconductors* 632 (World Scientific, 2012).
368. Catlow, C. R. A. & Stoneham, A. M. Ionicity in solids. *J. Phys. C Solid State Phys.* **16**, 4321 (1983).
369. Christensen, N. E., Satpathy, S. & Pawlowska, Z. Bonding and ionicity in semiconductors. *Phys. Rev. B* **36**, 1032–1050 (1987).
370. Tripathy, S. K. & Pattanaik, A. Optical and electronic properties of some semiconductors from energy gaps. *Opt. Mater.* **53**, 123–133 (2016).
371. Stroppa, A. & Peressi, M. ZnSe/GaAs (001) heterostructures with defected interfaces: structural, thermodynamic, and electronic properties. *Phys. Rev. B* **72**, 245304 (2005).
372. Hinuma, Y., Grüneis, A., Kresse, G. & Oba, F. Band alignment of semiconductors from density-functional theory and many-body perturbation theory. *Phys. Rev. B* **90**, 155405 (2014).

Acknowledgements
The authors thank L. van der Poll (former student in their group) for the photograph shown in Fig. 2b. This publication is part of the project Quantum Dots for Advanced Lightning Applications (QUALITy) with Project No. 17188 of the Open Technology Programme, which is (partly) financed by the Dutch Research Council (NWO).

Author contributions
The manuscript was written through contributions of all authors. All authors have given approval to the final version of the manuscript.

Competing interests
The authors declare no competing interests.

Additional information
Peer review information *Nature Reviews Materials* thanks Dongho Kim and the other, anonymous, reviewer(s) for their contribution to the peer review of this work.

Publisher's note Springer Nature remains neutral with regard to jurisdictional claims in published maps and institutional affiliations.

Springer Nature or its licensor (e.g. a society or other partner) holds exclusive rights to this article under a publishing agreement with the author(s) or other rightsholder(s); author self-archiving of the accepted manuscript version of this article is solely governed by the terms of such publishing agreement and applicable law.

© Springer Nature Limited 2023